W-AM-K7

ELECTROCHEMICAL CONTROL OF PROTEIN ADSORPTION AND ANTIBODY-ANTIGEN INTERACTION STUDIED BY TOTAL INTERNAL REFLECTION FLUORESCENCE

((**A.N. Asanov**[1,2], L.J. DeLucas[1], P.B. Oldham[2], and W.W. Wilson[2],))
[1]CMC@UAB, Birmingham, AL 35294; [2]MSU, Mississippi State, MS 39762

The objective of this work was to investigate the effect of electrochemical polarization on adsorption behavior of immunoglobulins on the surface of a transparent electrode. The mechanisms of immunoglobulin interactions with solid substrates as well as the ability to control interfacial behavior of antibodies are of great interest for such areas as immunoassays and immunobiosensors, drug release systems, chromatography, etc. Specifically, immobilized antibody activity and kinetics of antibody-antigen interactions depend on surface affinity, strength of adsorption, conformational changes and orientation of adsorbed molecules. In the present study the total internal reflection fluorescence (TIRF) technique in combination with a 3-electrode electrochemical system was used to monitor changes of immunoglobulin adsorption behavior and to probe polarization effect on the kinetics of antibody-antigen interactions. Rates of adsorption and desorption of immunoglobulins at the surface of a transparent SnO_2-electrode, reversibility of protein-surface binding, and structural rearrangements of adsorbed proteins were found to be strongly affected by externally applied polarization. Different electrochemical polarization programs allow modification of adsorption behavior of immunoglobulins and control of antibody-antigen interactions.

W-AM-K8

THEORY OF INTERACTION BETWEEN HELICAL BIOMOLECULES.

((A.A. Kornyshev[†] and **S. Leikin***)) [†]Institut für Energieverfahrenstechnik, Forschungszentrum Jülich, Germany and *LSB/DCRT and ODIR/NIDDK, NIH, Bethesda, MD 20892. (Spon. by D. C. Rau)

A large fraction of biomolecular interactions involves helices. In a number of cases forces have been directly measured (e.g. between DNA double helices, four-stranded guanosine helices, collagen, and some polysaccharides). While longer-range electrostatic double-layer forces are reasonably well understood, this is not so for the last 10-to-20 Å of separation, particularly when the net charge is small but the number of opposite charges on the helices is large (e.g. due to counterion binding). This work builds a theoretical foundation for understanding interactions between various types of helical molecules. In contrast to the traditional approximation of *cylinders* with constant charge density, we present exact analytic solutions for electrostatic and solvation forces between molecules with true *helical symmetry*, with inner cores inaccessible for water and with discrete charged (solvated) groups on them. We focus on the cases when drastic changes in attractive or repulsive interactions are caused by collective, symmetry driven effects. For example, the forces may be qualitatively different for helices with different number of strands, for helices with counter-charges lying on or between the strands, and even for helices with integer or non-integer number of charges per turn. The decay range of the force is often, but not always, determined by the helical pitch. We illustrate several more examples and discuss possible biological implications.

W-AM-K9

CALCULATION OF ASSOCIATION THERMODYNAMICS IN A MODEL PEPTIDE SYSTEM.

((**G.P. Brady** and K.A. Sharp)) University of Pennsylvania, Department of Biochemistry and Biophysics, Philadelphia, PA, 19104-6059. (Spon. by K.A. Sharp)

It has been known for decades that molecular binding is opposed by the famous "association entropy barrier", ΔS^{assn}, produced by the relative immobilization of the binding partners. The range of theoretical estimates of ΔS^{assn} is as large as the binding free energies themselves, while reliable experimental values are almost nonexistent. The present work provides a reliable experimental estimate of ΔS^{assn} for cyclic diglycine (cGG) and assesses of the suitability of current methods for computing binding thermodynamics. Calculations are based upon the decomposition of binding free energy into intra- and inter-molecular energy calculated using Molecular Mechanics, vibrational entropy calculated using Normal Mode Analysis, polar and nonpolar solvation, calculated using Finite-Difference Poisson Boltzmann and surface area free energy models respectively. We apply our procedure to the *gas* ↔ *crystal* ↔ *solution* phase equilibrium of cGG, the thermodynamics of which are known experimentally. Our solvation free energy (-16.4 kcal/mol) and sublimation enthalpy (-24.6 kcal/mol) agree with the experimental values to within 0.2 kcal/mol. The rigidity of cGG enables us to obtain a reliable estimate of -14 eu for the association entropy barrier to transfer of cGG from gas to the crystal. Subtracting exact expressions for S^{trans} and S^{rot} also gives us a reliable estimate of 41 e.u. for the entropy of the crystal lattice. We compute this lattice entropy using three different lattice models and demonstrate that the most rigorous model, Lattice Dynamics, is required to achieve reasonable agreement with the experimental value.

NONLINEAR OPTICAL MICROSCOPY: APPLICATIONS IN BIOLOGY

W-PM-SymI-1 **W. Zipfel, Cornell University**
Multiphoton Excitation of Intrinsic Fluorescence in Cells and in Intact Tissue

W-PM-SymI-2 **S. Fraser, California Institute of Technology**
Imaging Neuronal Targetting, Cell Migration and Synaptogenesis

W-PM-SymI-3 **E. Gratton, University of Illinois**
Mapping Membrane Microdomains and Observing Single Molecule Dynamics

W-PM-SymI-4 **W. Denk, Bell Laboratories, Lucent Technologies**
Functional Imaging of Neurons *in vitro* and *in vivo*

W-PM-SymII-1 **T. Gaasterland, Argonne National Labs and University of Chicago**
Strategic Analysis of Gene Sequence Data: From Sequence to Functional Networks

W-PM-SymII-2 **F. Cohen, University of California, San Francisco**
Exploring Multiple Sequence Information: Calculating Protein Structure and Function

W-PM-SymII-3 **S. Bryant, National Center for Biotechnology Information, National Library of Medicine**
Matching Sequence with Structure by Protein Threading

W-PM-SymII-4 **A. Sali, Rockefeller University**
From Sequence to Function by Comparative Protein Structure Modeling

ACTIN AND ACTIN BINDING PROTEINS

W-PM-A1

EFFECT OF PHALLOIDIN ON FORCE GENERATION AND PHOSPHATE RELEASE STEPS ((T. Wakabayashi, Y. Zhao*, M. Kawai*))
Dept of Physics, School of Science, University of Tokyo, Tokyo 113, Japan; *Dept of Anatomy, University of Iowa, Iowa City, IA 52242, U.S.A.

We treated chemically skinned rabbit psoas fibres with 18 μM phalloidin (PHA) in relaxing solution for 60 min, and monitored the force generation and phosphate (Pi) release steps by sinusoidal analysis:

$$\text{AM.ADP.Pi} \underset{k_{-4}}{\overset{k_4}{\rightleftharpoons}} \text{AM*ADP.Pi} \longleftrightarrow \text{AM*ADP + Pi} \quad (K_5)$$

where A=actin and M=myosin. The rate constants of the force generation step (k_4, k_{-4}) and the Pi association constant (K_5) were measured at pCa 4.65, (mM:) 0.5 Mg^{2+}, 5 MgATP, 0-32 Pi, 15 CP, 200 ionic strength (pH 7.0, 20°C), and the results obtained before and after the PHA treatment were compared. The results are summarized in the following Table.

	Units	Control	Phalloidin	PHA/Cont
k_4	s^{-1}	33±4	62±5	1.9
k_{-4}	s^{-1}	116±6	163±13	1.4
K_4		0.29±0.04	0.39±0.05	1.3
K_5	mM^{-1}	0.20±0.03	0.068±0.003	0.34

Thus, the effect is largest on K_5, and PHA weakens Pi association to cross-bridges by three fold. We also observed that PHA increases the rate constants of the force generation step (k_4, k_{-4}) and a slight increase in K_4. We conclude that the PHA binding to the thin filament may modify the conformation of actin, which in turn affects force generation and Pi release steps.

W-PM-A2

ACTIN CHANGES CONFORMATION WHEN IT BINDS NATURAL PROTEIN LIGANDS.
(P.D.J. Moens and C.G. dos Remedios) Muscle Research Unit, Dept. Anatomy & Histology, and Institute for Biomedical Research, The University of Sydney, Sydney 2006, Australia.

It has become conventional wisdom to consider the actin filament as a passive structure on which the "active" proteins such as myosin subfragment-1 exert their effects. We recently showed that fluorescence resonance energy transfer spectroscopy can be used to demonstrate reversible changes in the radial coordinate of probes which are covalently bound to the reactive Cys-374. Using 1,5-IAEDANS as a donor probe and DDPM as the non-fluorescent acceptor, we show that the probes (and by inference the position of Cys-374) increase their radial coordinate by about 4.5Å. This comparatively large movement is completely reversed in the presence of excess ATP. We have extended these experiments to include the effects of the Ca-regulatory proteins (tropomyosin-troponins) in the presence and absence of free Ca ions. We will also report the effects of caldesmon binding. These experiments raise fresh questions about a possible active role for actin in its interactions with these protein ligands.

W-PM-A3

BEHAVIOR OF A PYRENE-LABELED SUBDOMAIN 3/4 LOOP OF YEAST ACTIN: STRUCTURAL AND FUNCTIONAL INSIGHTS.
((L. Feng#, W.-L. Li#, E. Kim*, C. Miller*, E. Reisler*, and **P.A. Rubenstein#**))
#Dept. of Biochem., Univ. of Iowa, Iowa City, IA 52242 and *The Molec. Biol. Inst., UCLA, Los Angeles, CA 90095.

In the Holmes' F-actin model, a loop between subdomains 3 and 4 containing a hydrophobic plug at its tip has been proposed as an important determinant of actin helix stability. To characterize this loop in F-actin, we mutated S265 of yeast actin, adjacent to the plug, to a Cys (SC). To study the -SH groups separately, we made a second mutant (SCCA) by changing C374 of SC to Ala. Pyrene maleimide stoichiometrically labeled C265 and C374 of SC actin and only C265 or C374 of SCCA and WT actins, respectively. Both mutant actins, whether labeled or unlabeled, nucleated filament formation faster and polymerized to the same extent as WT actin. The fluorescence of co-polymerized labeled SCCA and WT actins was quenched in comparison with the sum of the fluorescence of each actin alone. Fluorescence quenching also occurred with SC F-actin. A new excimer band was observed in the co-polymer and in SC F-actin. Thus, the quenching was due to the interaction of the C-terminal probe on one monomer with the loop probe on another monomer. Further, the two Cys -SH groups had to be within about 18-19 A of one another, consistent with the Holmes model. Myosin S1 binding to SC and WT F-actins was similar. S1 caused an enhancement of loop pyrene fluorescence in SCCA actin, while binding of tropomyosin did not. In terms of the Holmes model, myosin binding to the outside of the filament caused a conformational change on the inside.

W-PM-A4

COLUMNAR LIQUID CRYSTALLINE PHASE OF F-ACTIN.
((J. X. Tang*, R. Oldenbourg^, J. A. Käs~, B. Millman#, and P. A. Janmey*))
*Brigham & Women's Hospital, Harvard Medical School, LMRC301, Boston, MA 02115. ^Marine Biological Lab, Woods Hole, MA 02543. ~Univ. of Texas at Austin, Austin, TX 78712. #Univ. of Guelph, Guelph, ON N1G 2W1.

F-actin is a filamentous assembly of the most abundant protein in every mammalian cell. It is a semiflexible biopolymer of 8-10 nm in diameter and has a persistence length of a few microns. We have observed in vitro spindles of F-actin, imbedded in a fluid background of suspension of orientationally ordered actin filaments, i. e., a nematic state of F-actin. Phase contrast microscopy shows these stable spindles of densely packed F-actin to be of various size in the order of 10 μm. The aspect ratio of long to short axes of the spindles is dependent on the average length of F-actin, and is approximately 5-10 for a mean filament length of 2 μm. The well defined surface of smooth curvature suggests active adjustments in the formation of these spindles. Further measurements of local birefringence by a pol-scope reveal that the optical birefringence is largely suppressed within the granules as opposed to the values of the surrounding nematic background. Low-angle X-ray diffraction through actin gels containing numerous, randomly oriented granules shows a clear ring corresponding to a basic spacing of 12 to 16 nm. Such a spacing corresponds to the packing of F-actin within the dense granules with interfilament separations less than the filament diameter, while the filaments in the surrounding fluid are much farther apart even though they still form an orientationally ordered phase. We propose that these spindles of F-actin are domains of a columnar liquid crystalline phase, co-existing with a nematic state of F-actin of a few percent in volume fraction.

W-PM-A5

STRUCTURE OF THE ACTIN:PROFILIN:RHODAMINE-PHALLOIDIN COMPLEX at 2.3 Å RESOLUTION.

((**Nancy Vogelaar**, Uno Lindberg*, Robert M.Sweet**, and Clarence E. Schutt)) Dept. of Chemistry, Princeton University, Princeton, NJ 08544, *Dept. of Zoological Cell Biology, Stockholm University, S-10691 Stockholm, Sweden, and **Dept. of Biology, National Sychotron Light Source, Brookhaven National Lab., Upton, NY 11973. (Spon. U. Lindberg)

Our laboratory has great interest in the conformational states of actin monomers and the roles they may play in determining filament properties. Actin, when cocrystallized with profilin, has been shown to undergo a large conformational change which is dependent on the composition of the crystal's soak solution. Two conformational states have been characterized by our lab, the "T-state"[1] which has a relatively narrow cleft between actin subdomains 2 and 4 and the "P-state" [2] which has a wide cleft between the subdomains as the result of rotations between subdomains 1 and 3 and 1 and 2. The current structure represents an intermediate between these two conformations, resembling the T-state, but with a rotation of subdomain 2 which opens the cleft. The refinement of this structure is incomplete and the rhodamine-phalloidin has not been located. It is anticipated that at the time of presentation, the phalloidin-binding site will have been determined. Because phalloidin binds only to actin filaments and not to actin monomers, identification of its binding site may prove an aid to filament modelling and provide structural insight into phalloidin's effect on actin polymerization and filament stability.

[1] C.E. Schutt, *et al.* (1993) Nature **365**, 810-816.
[2] J.K. Chik, *et al.* (1996) J. Mol. Biol., in press.

W-PM-A6

3D STRUCTURES OF F-ACTIN DECORATED WITH TWO DIFFERENT ACTIN-BINDING DOMAINS.

((**D. Hanein**, L.E. Rost, P. Matsudaira* and D.J. DeRosier)) Rosenstiel Basic Medical Sciences Research Center, Brandeis, University, Waltham, MA 02254 ; and *Whitehead Institute for Biomedical Research, Massachusetts Institute of Technology, Cambridge, MA 02142.

The state of actin is a function of its association with actin binding proteins. Actin binding proteins are often bivalent molecules that can crosslink actin to form gels or bundles *in vitro* and *in vivo*. The actin bundles found in the microvilli of the intestinal brush border contain the bundling proteins fimbrin and villin.

Fimbrin belongs to a superfamily of actin cross-linking proteins that share homologous 27-kDa actin-binding domains. The three-dimensional structures of actin filaments and of actin filaments decorated with fimbrin (N375) were determined to 28Å resolution using electron cryo-microscopy and image analysis. The N375 consists of the N-terminal 27-kDa actin binding domain and a pair of calmodulin-like calcium binding sites. N375 contacts the outer surface of subdomain 1 and subdomain 2 of one actin monomer and subdomain 1 of the neighboring monomer along the long-pitch helix. Actin residues 43-100 from one monomer and 350-355 on the adjacent monomer form a surface that makes extensive interactions with N375. We observe changes near the N- and C-termini and in subdomains 4 and 2 in the actin. The structural and biochemical results presented in this paper confirm the existence of a common actin-binding site to a homologous conserved 27-kDa actin binding and suggest that the binding of N375 is accompanied by a conformational change in actin.

Villin belongs to a different class of proteins, which can bind and sever actin filaments. Unlike other members of its class, villin has a second and unique actin binding domain, which enables it to bundle actin filaments. This second actin binding domain termed villin headpiece, is a 76 residue region at the C terminal end of the molecule. In three-dimensional reconstructions from electron micrographs, the villin headpiece appears to bind away from the fimbrin (N375) site and near the phalloidin site on actin.

W-PM-A7

3-D RECONSTRUCTION OF SMOOTH MUSCLE THIN FILAMENTS: CONTRIBUTION OF CALDESMON AND CALPONIN TO FILAMENT STRUCTURE.

((J.L. Hodgkinson[1,2,4], M. El-Mezgueldi[1], S. Marston[1], R. Craig[2], P. Vibert[3], & W. Lehman[4]))
[1]Imperial College Sch. Med., Natl. Heart & Lung Inst., London, UK SW3 6LY; [2]Dept. Cell Biology, Univ. Mass. Med. Sch., Worcester MA 01655; [3]Roscastiel Ctr., Brandeis Univ., Waltham MA 02254; [4]Dept. Physiology, Boston Univ. Sch. Med., Boston MA 02118.

The structural organization of smooth muscle tropomyosin, caldesmon and calponin on F-actin was analyzed by three-dimensional image reconstruction of negatively stained filaments. When calponin was added to actin or actin-tropomyosin filaments (1 calponin: 1-2 actin), it was directly visualized as a compact mass with a shield-like appearance. The protein was located over sub-domain 2 of actin and connected to adjoining actin monomers along the long pitch actin helix. Fitting the reconstructions to the atomic model of F-actin indicates that calponin is associated with residues near the N-terminus and a loop projecting from the C-terminus (residues 349-352) of one actin monomer and also with residues 92-95 of the actin directly below in the long pitch helix. Tropomyosin was observed to be located on the outer edge of the inner actin domain in actin-tropomyosin-calponin filaments and on the inner edge of the outer domain in actin-tropomyosin controls. When caldesmon C-terminal fragment 606C (residues 606-756) was added to actin-tropomyosin (~1 606C: 3 actin, which *in vitro* inhibited acto-S-1 ATPase by ~80%), tropomyosin was also localized on the outer edge of the inner domain of actin (*cf.* Vibert *et al.*, 1993). 3-D reconstruction did not reveal the location of the 606C-fragment clearly, either because the stoichiometry was too low or because the 606C was disordered or not compact enough under our conditions; weak density, possibly due to 606C, was associated with the underside of actin sub-domain 1. Given the locations of caldesmon and calponin and the known binding of myosin S-1, each should compete with the others for binding to actin. The results also indicate that neither caldesmon nor calponin control tropomyosin position in the same way as does troponin.

W-PM-A8

INTERACTION BETWEEN EXPRESSED NEBULIN FRAGMENTS AND ACTIN.

((**J.Q. Zhang** and R. Horowits)) NIAMS, NIH, Bethesda, MD 20892.

cDNA clones encoding mouse skeletal muscle nebulin (Zhang et al., Eur. J. Biochem. 239: 835, 1996) were expressed in E. coli as thioredoxin fusion proteins and purified in the presence of 6 M urea. These fragments, called 7a and 8c, contain 28 and 19 of the weakly repeating ~35 residue nebulin modules, respectively. The modules are arranged into more highly conserved nebulin super repeats composed of 7 modules. The nebulin fragments are soluble at extremely high pH, but aggregate when dialyzed to neutral pH as assayed by centrifugation at 16,000xg. However, when mixed with varying amounts of G-actin at pH 12 and then dialyzed to neutral pH, the nebulin fragments are solubilized in a concentration dependent manner, remaining in the supernatant along with the monomeric actin. These results show that interaction with G-actin allows the separation of apparently insoluble nebulin aggregates from soluble actin-nebulin complexes by centrifugation. We used this property to assay the incorporation of nebulin fragments into preformed actin filaments. Varying amounts of aggregated nebulin were mixed with a constant amount of F-actin at pH 7.0. The nebulin aggregates were pelleted by centrifugation at 5200xg, while the actin filaments, including incorporated nebulin fragments, remained in the supernatant. Using this assay, we found that nebulin fragments 7a and 8c bound to actin filaments with high affinity. In addition, we found that fragment 7a binds to F-actin with a stoichiometry of one nebulin module per actin monomer, the same stoichiometry we found *in vivo*. In contrast, 8c binds to F-actin with a stoichiometry of one module per two actin monomers. These data indicate that 7a can be incorporated into actin filaments to the same extent found *in vivo*, and suggest that shorter fragments may not bind actin filaments in the same way as the native nebulin molecule.

W-PM-A9

COMPLETE CODING SEQUENCE OF HUMAN CARDIAC NEBULETTE.

((**Carole L. Moncman** and Kuan Wang)). Dept. of Chemistry and Biochemistry, University of Texas at Austin, Austin, TX, 78712.

Nebulette is a 107 kD nebulin-like protein found in the I-Z-I complex of cardiac myofibrils (Cell Motil & Cytoskel. 32: 205-225). We have cloned and sequenced 6 kb of the 8 kb nebulette transcript; this contig contains the complete coding sequence, as well as portions of the untranslated regions. From the deduced primary structure, nebulette is composed of four domains: an acidic N-terminal domain (85 aa), a large nebulin-like repeat domain (760 aa), a linker domain (107 aa) and a Src homology 3 domain (55 aa). The N-terminal domain appears to be unique to nebulette; while the latter three domains share striking sequence conservation with the C-terminal 100 kD of nebulin. The repeat domain is composed of 22 nebulin-like 35 residue modules, that closely resemble the single repeat modules near the carboxyl terminus of skeletal muscle nebulin. The presence of both the nebulin-like modules and the Src homology 3 domain suggest that this protein serves as an actin binding protein in cardiac muscle. In addition, these domains may act to target both nebulette and nebulin to the Z-line of the myofibrils. Immunofluorescent localization studies on spreading cardiomyocytes in culture suggest that this protein may be involved in early assembly events during myofibrillogenesis. To investigate the roles of the nebulette domains in the function and assembly of this protein in the cardiac muscle, we have engineered and expressed recombinant proteins containing either the individual domains or combinations of these domains as fusions with GFP in eukaryotic cells. The expression and assembly of the recombinant proteins is being investigated by fluorescence microscopy

(Supported by grants from USDA and NIH).

W-PM-B1

UV MODIFICATION OF TRYPTOPHAN RESIDUES ALTERS OPENING EFFICACY OF CYCLIC NUCLEOTIDE-GATED CHANNELS. ((**T.R. Middendorf**[1], C. Warren[2], C. Adams[2], D.A. Baylor[1] and R.W. Aldrich[2])) [1]Dept. of Neurobiology and [2]Dept. of Molecular and Cellular Physiology and Howard Hughes Medical Institute, School of Medicine, Stanford University, Stanford, CA 94305.

We have measured the effects of *in situ* UV modification of channels to probe the role of aromatic amino acids in ion channel function. UV irradiation of excised membrane patches from *Xenopus* oocytes expressing cyclic nucleotide-gated (CNG) rod channels caused a dose-dependent, irreversible decline in patch current at saturating ligand concentrations. This behavior is consistent with permanent chemical modification of amino acids in the channel. As the excitation wavelength was longer than 250 nm, the UV light was absorbed only by the sidechains of Trp, Tyr, and Phe residues. The wavelength dependence of the UV sensitivity indicated that current knockout is initiated by Trp absorption. To identify the specific Trp residue(s) involved, a series of point mutants, each lacking one of the ten Trps present in the wild type rod channel, was constructed. The UV sensitivities of these mutants suggest that photochemical modification of Trp 353, located in the channel pore, is primarily responsible for the current knockout.

Factors influencing the UV sensitivity were also investigated. The UV sensitivity was lower when: i) 10 uM Ni^{++} was present on the cytoplasmic face of the patch, ii) olfactory, rather than rod, CNG channels were irradiated, and iii) cGMP rather than cAMP was used to activate the currents. These findings suggest a mechanism for the effect: irradiation decreases patch current by lowering the efficacy of channel opening.

(Supported by EY01543, EY06351, the McKnight Foundation, and the Howard Hughes Medical Institute.)

W-PM-B2

FUNCTIONAL ARCHITECTURE OF THE LIGAND BINDING DOMAIN OF CYCLIC NUCLEOTIDE-GATED CHANNELS ((**M. D. Varnum** and W. N. Zagotta)) Dept. of Physiology and Biophysics and Howard Hughes Medical Institute, University of Washington, Seattle, WA 98195.

Cyclic nucleotide-gated (CNG) ion channels of retinal photoreceptors and olfactory neurons are presumably tetrameric complexes containing four cyclic nucleotide-binding sites. Cyclic nucleotide binding to these sites induces a conformational change that is translated into channel opening at the pore. We are investigating the regions of the CNG channel sufficient for ligand binding and necessary for communication of binding to other channel domains. Deletion mutations in the cDNA of the bovine rod CNG channel followed by expression in Xenopus oocytes indicated that amino acids 572-621, but not amino acids 608-682, were necessary for cyclic nucleotide-dependent channel activity. Rod Δ608-682 channels displayed agonist efficacies and apparent affinities for cGMP and cAMP similar to wild-type channels, suggesting that the deleted domain does not play a fundamental role in channel activation. Using bacterial expression and affinity purification, we have isolated various COOH-terminal channel domains. We have observed specific binding of ^{3}H-cGMP to recombinant CNG channel protein encompassing amino acids 497-690. These results suggest that amino acids 497-607 of the channel are sufficient for ligand binding. Isolated CNG channel domains provide a means of determining the binding affinity for cyclic nucleotides independent of coupling to the conformational change at the pore. Furthermore, they may permit determination of the functional symmetry of the channel at the level of the binding domain, and of the intersubunit and interdomain interactions underlying CNG channel activation.

W-PM-B3

ALTERED GATING OF HETEROMULTIMERIC OLFACTORY CYCLIC NUCLEOTIDE -GATED CHANNELS BY THE THE ß SUBUNIT. ((**M.S. Shapiro** and W.N. Zagotta)) Dept. Physiol./Biophysics and Howard Hughes Medical Institute, University of Washington, Seattle WA 98195.

We studied cloned rat olfactory cyclic nucleotide-gated channels expressed in Xenopus oocytes and T201 cells in inside-out patches. Co-expression of α+ß subunits produced heteromultimeric channels with different gating properties than homomultimeric α channels. For α+ß channels, the dose-response relation for cAMP had a half-saturating concentration ($K_{1/2}$) that was ~5-fold lower than for α channels, but the relations for cGMP were similar, and the fitted Hill slopes were reduced (~1.4 vs. ~2.2). α+ß currents expressed in oocytes, but not T201 cells, desensitized with a time constant of several seconds to about half the initial current. These results are consistent with previous work (Bradley et al., *PNAS* 91:8890-8894; Liman and Buck, *Neuron* 13:611-621). Like that for cAMP, the dose-response relation for cIMP for α+ß channels had a $K_{1/2}$ ~5-fold lower than for α channels ($K_{1/2}$= 86 μM vs. 406 μM at 60 mV and $K_{1/2}$= 117 μM vs. 477 μM at -60 mV). For both α and α+ß channels, the maximum current at saturating cAMP, cGMP and cIMP were similar but the $K_{1/2}$ for cIMP was ~7-fold higher than for cAMP. These results suggest that both channels have a high equilibrium constant for opening of ligand-bound channels for all three ligands, and that cIMP has the highest $K_{1/2}$ because it has an especially low initial binding affinity. The ligand-dependent nature of the dose-response relation changes suggests a large influence of the ß-subunit cyclic nucleotide-binding region. Consistent with that idea, chimeric ß subunits with the α cyclic-nucleotide-binding region, co-expressed with wild-type α subunits in oocytes, gave non-desensitizing currents with $K_{1/2}$ for all three ligands similar to α channels, but Hill slopes similar to wild-type α+ß currents. Wild-type ß subunits and the chimeric ß/α subunits, expressed alone, did not produce measurable currents.

W-PM-B4

A STATE-DEPENDENT CONFORMATIONAL CHANGE IN THE PORE OF CYCLIC NUCLEOTIDE-GATED CHANNELS. (**A.A. Fodor**, S.E. Gordon and W.N. Zagotta) Dept. of Physiology and Biophysics and Howard Hughes Medical Institute, Univ. of Washington, Seattle, WA 98195.

Ion channels directly gated by cyclic nucleotides are key players in visual and olfactory signal transduction. We examined the effects of the local anesthetic tetracaine on rod and olfactory cyclic nucleotide-gated channels formed from subunit 1 expressed in Xenopus oocytes. We found that tetracaine on the intracellular face of excised patches effectively blocked the bovine rod channel but not the rat olfactory channel at saturating concentrations of cGMP. The difference in apparent affinity between the rod and the olfactory channel could be explained by the rod channel spending more time in a closed state at saturating cGMP compared to the olfactory channel. Tetracaine bound with higher affinity to this closed state and hence was a more effective blocker of the rod channel. Furthermore, tetracaine became more effective at low concentrations of cGMP and at saturating concentrations of cAMP, conditions which permit the channel to spend more time in closed states. Tetracaine block was more effective at depolarized voltages, consistent with a pore block hypothesis. These data indicate that tetracaine is a state-dependent pore blocker suggesting that the inner mouth of the pore of cyclic nucleotide-gated channels undergoes a conformational change during channel opening.

W-PM-B5

COVALENT ACTIVATION OF CYCLIC NUCLEOTIDE-GATED ION CHANNELS BY SULFHYDRYL-REACTIVE DERIVATIVES OF CYCLIC GMP ((**R. Lane Brown** & Tammie L. Haley)) R.S. Dow Neurological Sciences Institute, Portland, OR 97209

First discovered in the sensory epithelium of the visual and olfactory systems, cyclic nucleotide-gated ion channels are now known to play a key role in signaling processes throughout the body. These channels are composed of distinct α and β subunit types. We have found that treatment of excised patches containing expressed rod α-subunit channels with sulfhydryl-reactive iodoacetamide or vinylsulfone derivatives of cGMP resulted in irreversible activation. These persistent currents were sensitive to both Mg^{2+} and tetracaine. Pretreatment with the sulfhydryl-modifying reagents NEM and DTNB significantly blocked covalent activation. The blocking effect of DTNB was reversed by treatment with DTT. These results suggested that covalent activation resulted from the covalent tethering of cGMP to channel binding sites by reaction with an endogenous cysteine. We are now attempting to identify the site of attachment using site-directed mutagenesis. Of the six cysteine residues present in the α subunit, four are proposed to lie on the cytoplasmic face of the channel: the first, C35, lies near the N-terminus of the protein; the second, C481, is located between the final transmembrane segment of the channel and the cyclic nucleotide-binding site; the final two, C505 and C573, lie within the cyclic nucleotide-binding site. Both C481 and C505 have been eliminated as viable candidates for the site of attachment because conversion of either residue to a non-reactive amino acid did not prevent covalent activation. The ability to target specific subunits for covalent attachment of cGMP will allow us to generate channel populations with a defined complement of ligands. This technique will provide us with a unique opportunity to study the allosteric mechanism of channel activation and to examine the individual properties of each subunit type present in a heteromeric channel. (Supptd. by EY11097)

W-PM-B6

LOCKING SINGLE cGMP-GATED CHANNELS INTO PARTIALLY LIGANDED STATES. ((**ML. Ruiz** and J.W. Karpen)) Dept. of Physiology, University of Colorado School of Medicine, Denver, CO 80262

In retinal rod outer segments only about 1% of the cGMP-gated channels are active at physiological cGMP concentrations. Since each of four channel subunits possesses a cGMP binding site, it is thought that many channels are partially liganded, and may give rise to subconductance states. To understand the steps involved in channel activation, we have developed a method for locking single channels into partially liganded states. Cloned bovine retinal cGMP-gated channel α subunits were expressed in *X. laevis* oocytes. Single channel patches were perfused with a photolyzable analog of cGMP called 8-*p*-azidophenacylthio-cGMP. Short exposures to UV light caused the analog to covalently attach to cGMP binding domains on the channel. After extensive washing of the patch in a solution lacking free cGMP, some channels opened spontaneously with low probability appropriate for a partially liganded channel. Dose response relations measured before and after exposures revealed shifted curves after photolysis with lower $K_{1/2}$ values and lower Hill coefficients. Longer exposure to UV light resulted in a fully liganded channel that opened with maximum probability, (addition of free cGMP had no effect). Under conditions that favor low levels of covalent liganding, channels mostly opened to sub-conductance states. Moreover, with a channel locked in a particular liganded state (in the absence of free cGMP) opening was not restricted to a single subconductance level. Instead, such a channel was able to move between different subconductance levels. This method allows us to study individual binding events in isolation in order to formulate a more complete model of channel activation. In the future we will use this method on channels formed from α and β subunits. Supported by NIH grant EY09275.

W-PM-B7

GATING OF CYCLIC-NUCLEOTIDE GATED CHANNELS BY VOLTAGE AND PERMEANT ION. (**F. Sesti** & E. Eismann) IBI, Forschungszentrum Jülich, Postfach 1913, D-52425 Jülich

Cyclic nucleotide-gated (CNG) channels are only weakly voltage-dependent, although they display significant homology with voltage-gated channels. We now show that, under certain experimental conditions, in addition to ligand control, CNG channels have retained their ability to respond to changes in membrane voltage. Monovalent cations suppress this voltage dependence under physiological conditions by binding to glutamate residues within the pore. This ion binding mechansim restricts gating control exclusively to the binding of cyclic nucleotides and may represent an evolutionary step to eliminate the voltage-dependence of an ancestral channel.

W-PM-B8

RESIDUES 533 AND 596 AFFECT NUCLEOTIDE SPECIFICITY AND RELATIVE AFFINITY OF THE BOVINE RETINA CYCLIC NUCLEOTIDE GATED CHANNEL. ((**S-P. Scott** and J.C.Tanaka)) University of Pennsylvania, School of Dental Medicine, Philadelphia, PA 19104

Previously, we suggested that the coordination of Phe 533 on β5, Thr 560 on β7 and Lys 596 and Asp 604 on the C αhelix in the binding site of the cyclic nucleotide gated channel (CNGC) contribute to nucleotide specificity and selectivity. Mutagenesis by others demonstrated the involvement of residues 560 and 604 in nucleotide interactions within the binding site. We generated single and double mutants at 533, 596 and 604 in the bovine retina CNGC which provide experimental support for the involvement of these residues. A K596R mutant expressed in COS-1 cells had a $K_{0.5}$ (concentration producing half maximal current) of 37 μM for cGMP, compared to 27 μM in wild type. K596R did not bind cAMP whereas the wild type had a $K_{0.5}$ of >1 mM and produced 40% of the current at saturating cGMP concentrations. A D604Q mutant produced no current with 10 mM cAMP and small currents with 10 mM cGMP. In contrast, a K596R:D604Q double mutant had $K_{0.5}$'s of 54 and 211 μM for cGMP and cAMP, respectively. cAMP activated <15% of the maximal current. A mutant F533Y/K596R had a $K_{0.5}$ of 20 μM and 380 μM for cGMP and cAMP, respectively, and cAMP elicited 40% of maximal cGMP current. We conclude: 1) The single mutant K596R does not bind cAMP whereas the double 596 mutants are more sensitive to cAMP than is wild type. 2) Residues 533, 596 and 604 act in concert and no single residue dominates ligand coordination. 3) Molecular modeling sucessfully predicted the involvment of these residues in ligand interactions.

BILAYERS - PROBES AND DYNAMICS

W-PM-C1

HOW CAN MECHANOCHEMICAL PROPERTIES OF LIPID BILAYER VESICLES BE SIMULATED BY MONOLAYERS AT THE AIR-WATER INTERFACE? ((Si-shen Feng and Robert C. MacDonald)) Department of Chemical Engineering, National University of Singapore, Singapore 119260 and Department of BMBCB, Northwestern University, 2153 North Campus Drive, Evanston, IL 60208.

We present a theoretical analysis for the lipid monolayer-bilayer correspondence problem, which illuminates the conditions under which a monolayer at the air-water interface and one leaflet of a bilayer vesicle are mechanochemically equivalent and also provides a procedure to determine from the monolayer's π-a relationship the thermodynamic and mechanical properties of the monolayer and bilayer vesicles. The difference between a monolayer at the air-water interface and one half of a bilayer is that the former but not the latter exhibits a microscopic interfacial tension at the interface between the air and the hydrocarbon chains of the monolayer. It is revealed that a monolayer comes into equilibrium with bilayer vesicles at a monolayer pressure that is equal in magnitude to the microscopic interfacial tension between water and the monolayer, which is proved to be the same as the collapse pressure of the monolayer in compression. For the first time, procedures are described to obtain analytically from a theoretical or empirical equation of state of a monolayer, or graphically from the π-a curve of the monolayer, a variety of thermodynamic properties of the monolayer and bilayer vesicles, in particular, surface free energy, surface chemical potential and thermodynamic activity of the constituent lipid molecules. The method is exemplified for the monolayer and bilayer vesicles of dilauroyl phosphatidylethanolamine. (Supported by NIH 1 P01 HL45168)

W-PM-C2

STEADY-STATE LATERAL ORGANIZATION OF LIPID MEMBRANES WITH ACTIVE INTEGRAL PROTEINS

M. C. Sabra and O. G. Mouritsen
Department of Chemistry, Technical University of Denmark
Building 206, DK-2800 Lyngby, Denmark

A generic model is proposed to describe the steady-state organization of a binary lipid bilayer incorporated with active integral membrane proteins. Each protein can assume two different hydrophobic lengths corresponding to two energetically distinct conformational states that couple to the surrounding lipid bilayer in a way that depends on the hydrophobic matching. The proteins are excited (driven) by an influx of energy which is dissipated to the lipid bilayer by a series of processes that involve de-exicitation and lateral redistribution of the proteins, restructuring of the lipid matrix, and conformational changes in the lipids. The resulting steady-state lateral organization of a driven lipid-protein membrane characterized by this model is described in case of an integral protein in a DMPC-DSPC lipid bilayer.

W-PM-C3

DEHYDROERGOSTEROL STRUCTURAL ORGANIZATION IN A MODEL SYSTEM OF MEMBRANES **((Luís M. S. Loura and Manuel Prieto)) CQFM, Complexo I, IST, Av. Rovisco Pais, 1096 Lisboa Codex, Portugal**

The aggregation of $\Delta^{5,7,9(11),22}$-ergostatetraen-3β-ol (dehydroergosterol or DHE), a fluorescent analogue of cholesterol, was studied in phospholipid vesicles by measuring the fluorescence anisotropy of samples having varying sterol:lipid ratios. The organization of DHE in these model systems of membranes is strongly dependent on the vesicles type. In small unilamellar vesicles (SUV), no evidence for aggregation is obtained and the fluorescence anisotropy is rationalized on the basis of a random distribution of fluorophores. On the contrary, in large unilamellar vesicles (LUV), a steeper concentration depolarization was observed. In order to explain this, a model which takes into account transbilayer dimer formation was derived. This was further confirmed from observation of excitonic absorption bands of 22-(NBD, *N*-7-nitrobenz-2-oxa-1,3-diazol-4-yl-amino)-23,24-bisnor-5-cholen-3β-ol (NBD-cho-lesterol) in LUV, which disappear upon sonication. It is concluded that, in agreement with recent works, sterol aggregation is an efficient process in large vesicles (and probably in natural membranes), even at low concentrations (~5 mol%). **(Supported by JNICT, programs PUEM/S/ERC/53/93 and PECS/C/SAU/144/95. L. M. S. L. acknowledges a grant (BD 3927/94) from PRAXIS XXI.)**

W-PM-C4

MAGNETICALLY ALIGNED LANTHANIDE-DOPED PHOSPHOLIPID BILAYERS: THE IDEAL SYSTEM FOR THE STUDY OF MEMBRANE PROTEIN STRUCTURE BY SOLID STATE NMR AND LOW-ANGLE DIFFRACTION.
((R.S. Prosser* and R.R. Vold)) Department of Chemistry and Biochemistry, University of California at San Diego, La Jolla, CA, 92093-0359. *Present Address: Department of Chemistry and the Liquid Crystal Institute, Kent State University, Kent, OH 44242.

Long- and short-chain phospholipids may be combined in solution to form a diskoidal mesogenic unit in which the planar bilayer center, occupied by the long-chain lipid, is edge stabilized by the short chain lipid (Sanders and Schwonek, *Biochemistry* 31:8898, 1992). The aggregate may be doped with either Eu^{3+}, Er^{3+}, Yb^{3+}, or Tm^{3+} lanthanide ions resulting in a bilayer assembly with a net positive diamagnetic anisotropy, $\Delta\chi$. In this case, the bilayer normal aligns along the applied magnetic field, allowing the acquisition of well-resolved solid state NMR spectra for membrane proteins in any motional regime. At certain temperatures and lanthanide concentrations, a smectic bilayer phase has been identified by low angle diffraction. Details of the physical properties of this system and its potential for study of membrane protein structure by various techniques will be presented.

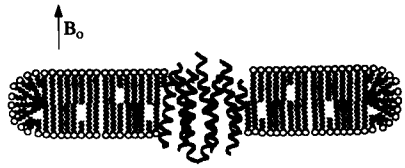

W-PM-C5

EFFECT OF WATER STRUCTURE ON THE PARTITIONING OF SOLUTES AND ON MOLECULAR ORGANIZATION IN MICELLES AND BILAYERS
((**S. Schreier**, D. Perigo, G.S.S. Ferreira, F. Casalanovo and R.S. Teixeira)), Institute of Chemistry, Universidade de Sao Paulo, C.P. 26077, S. Paulo, 05599-970, Brazil (Spon. A.S. Ito)

Ions of the Hofmeister series and urea are known to alter water structure and, as a consequence, the solubility of molecules in the aqueous medium, as well as their distribution between this medium and organic solvents. Moreover, these additives have been shown to affect organizational properties of lipid bilayers and detergent micelles by a multi-component mechanism, including direct binding. We have examined the effect of kosmotropic (increase water structure, SO_4^{2-}, HPO_4^{2-}, Cl^-) and of chaotropic (decrease water structure, SCN^-, ClO_4^-) anions and of urea (chaotropic) on the aqueous solubility and partitioning of the charged and uncharged forms of the local anesthetic tetracaine (TTC) into zwitterionic lipid bilayers (egg phosphatidyl choline) and detergent micelles (N-hexadecyl-N,N-dimethyl-3-ammonium-1-propane sulfonate). Fluorescence measurements indicated that, while the kosmotropes decreased water solubility and increased binding of charged and uncharged TTC to the membrane-like environment, the chaotropes had the opposite effect. Spin labeling EPR and quasielastic light scattering showed that the additives interact with both bilayers and micelles, leading to changes in structure and size of the aggregates. Nevertheless, while the changes in partitioning correlate very well with the effect of the additives on water structure, they do not bear a relationship with the latter effects.
Supported by FAPESP, CNPq, CAPES.

W-PM-C6

HEAT EVOLUTION OF VESICLES ⇌ MICELLES TRANSITIONS IN MIXTURES OF PHOSPHOLIPIDS AND SURFACTANTS.
((Ella Opatowski, Michael Koslow and **Dov Lichtenberg**)) Dept. of Physiology and Pharmacology, Tel-Aviv University, Sackler Faculty of Medicine, Tel-Aviv, ISRAEL.

The heat associated with vesicle ⇌ micelles transitions in mixtures of bilayer-forming phospholipids and micelle-forming surfactants is a complex function of the difference between the chemical potentials of each of the components in bilayers, mixed micelles, and surfactant monomers.
When a titration step in an isothermal titration calorimeter (ITC) results in extraction of Δn_{mono} from mixed aggregates and in transformation of Δn^L and Δn^D molecules of lipid and surfactant, respectively, from mixed micelles into vesicles, the heat evolution is :
$\Delta Q = \Delta n_{mono} \cdot \Delta H_{ext} + \Delta n^L \Delta H^L + \Delta n^D \Delta H^D$
where ΔH_{ext}, ΔH^L and ΔH^D are the respective molar enthalpies.
The values of Δn_{mono}, Δn^L and Δn^D are complex but descrete functions of the phase boundaries in the system and the detailed protocols of mixing lipid with surfactant.
We have formulated a method for evaluation of each of the ΔH values separately from the combined results of ITC experiments carried out under various mixing protocols.
For phosphatidylcholine-otylglucoside mixtures, we found
ΔH_{ext} = -1.7 Kcal/mole, ΔH^D = 0.65 Kcal/mole and ΔH^L = -0.59 Kcal/mole.
These results are consistent with the spontaneous curvatures of the lipid and surfactant, for which the ΔH values can thus serve as a quantitative measure.

W-PM-C7

USE OF RECEPTOR-LIGAND INTERACTIONS TO PROBE THE DYNAMICS OF FLUID-LIKE INTERFACES
((**D. Leckband** and C. Yeung)) University of Illinois at Urbana-Champaign, Champaign, IL 61801

Lipid bilayers are dynamic, fluidlike structures. It has been proposed that structural and dynamic entropic forces dominate the short-range interactions between lipid membranes. We demonstrated by direct force measurements that these short-range repulsive forces also impede the protein binding to immobilized receptors. In this work, we have used the sensitivity of streptavidin-biotin recognition to short-range steric forces, in order to probe the dynamics of lipid membranes. The biotin is bound to the membrane via a lipid anchor, and therefore undergoes similar mobility to the matrix lipids. We used the time-dependent adhesion between the membranes to investigate the dynamics of lipid mobilities. With this approach we have measured both slow and rapid lipid fluctuations on the membrane surface. The slow movement is due to constrained lateral mobility in the bilayer. However, the fast process is attributed to lipid (biotin-lipid) protrusions from the membrane in the presence of the protein active site. On the basis of temperature dependent measurements, we determined the activation energy associated with the slow process, and the temperature dependence of the fast process.

W-PM-C8

KINETICS OF SOLUTE RELEASE FROM LIPID VESICLES INDUCED BY SWELLING
((E.Spiazzi, S. Giner, and E.A. Disalvo)) CIDCA, University of La Plata, Faculty of Pharmacy and Biochemistry, University of Buenos Aires, Argentina.

A set of transport equations addressed to explain the leakage of trapped solutes occurring during vesicle swelling is derived.
The volume increase involves water and solute fluxes together with the development of mechanical tensions in the membrane. The final equilibrium is achieved when the mechanical and chemical forces are counterbalanced. To analyze the dynamics of the transport in correlation to the changes in the membrane tension, the viscoelastic properties of the membrane were coupled to the chemical gradients introducing a mechanochemical potential. The volume increase creates a mechanical elastic stress opposing to the water influx. This makes the internal pressure of the liposome higher than that of the outer solution, and opposes to the influx of matter. We analyze the situation in which chemical gradients of non charged solutes combined with mechanical stress gradient (i.e. non zero tensions) can produce changes in the membrane barrier properties allowing the release of molecules trapped in the internal volume. The resolution of the equation system allows to explain the behavior of selective and non selective membranes. By monitoring the evolution in time of the vesicle volume, the amount of trapped solute and its concentration the evolution of membrane permeability properties produced by swelling can be evaluated.

With funds from UBACyT and Fundacion Antorchas

W-PM-C9

TRANSITION FROM SOLUBILITY-DIFFUSION TO POROUS MEMBRANE PERMEATION MECHANISM INDUCED BY OSMOTIC SWELLING.
((G. **Benzal**, A.C. Biondi de Lopez and E.A. Disalvo)) Instituto de Fisicoquímica, U. N. de Tucumán; Química General e Inorgánica, Facultad de Farmacia y Bioquímica, U. de Buenos Aires, Argentina.

Two mechanisms for the permeation of solutes across lipid bilayers have been proposed: solubility-diffusion and transient pores. Both, consider the transport process to take place in a static membrane in the absence of membrane tensions. In this paper, a model considering the shift from the solubility-diffusion to a porous mechanism as a consequence of swelling is presented. The membrane tension generated by the swelling of vesicles subject to a hypotonic stress may promote a decrease in the cohesive forces between the lipids of the bilayer. Under these conditions, the probability of formation of transient pores, through which water soluble molecules can diffuse out of the vesicle, is greatly increased. Water soluble molecules of different sizes can diffuse out of the vesicle according to the probability of forming pores matching the respective solute radius at each stage of swelling. The creation of pores of longer mean life is proportional to the amount of water entering the bilayer. The diffusion of trapped solute, used as a probe to measure the transition between solubility to porous membrane, is produced at a water in lipid ratio 2.5:1 which is comparable to that found when the bilayer goes from the gel to the liquid crystalline state. Above this ratio, the area increase upon swelling predicts a lipid in water ratio that accounts for the bilayer disruption. *(With funds of UBACyT, Fundación Antorchas and U. · Tucumán)*

W-PM-C10

IN VIVO GENE ELECTROINJECTION AND EXPRESSION IN RAT LIVER.
((R. Heller[1], M. Jaroszeski[1], A. Atkin[2], D. Moradpour[3], R. Gilbert[1], J. Wands[3] and **C. Nicolau[2]**)) [1]Univ. South Florida, Tampa, FL 33612; [2]CBR Labs, Harvard Medical School, Boston, MA 02135; [3]Mass. General Hospital, Harvard Medical School, Charlestown, MA 02129.

In vivo targeted gene transfer by non-viral vectors is subjected to anatomical constraints depending on the route of administration. Transfection efficiency and gene expression in vivo using non-viral vectors is also relatively low. We report that in vivo electropermeabilization of the liver tissue of rats in the presence of genes encoding luciferase or ß-galactosidase resulted in the strong expression of these genetic markers in rat liver cells. About 30-40% of the rat liver cells electroporated expressed the ß-galactosidase genetic marker 48 h after electroporation. The marker expression was also detected at least 21 days after transfection at about 5% of the level 48 h after electroporation. The results indicate that gene transfer by electroporation in vivo may avoid anatomical constraints and low transfection efficiency. The total number of transfected cells in our experiments is limited only by the geometry of the applied electrical field.

W-PM-D1

MUTATIONAL ANALYSIS OF L-TYPE CA^{2+} CHANNELS REVEALS DISTINCT REGULATORY SITES FOR NEUTRAL AND CHARGED DIHYDROPYRIDINE (DHP) DERIVATIVES. ((L. Lacinova[2], **R-H. An**[1], F. Hofmann[2], D.J. Triggle[3], and R. S. Kass*[1])) Dept. of Pharmacology. Columbia University, New York, NY 10032[1]; Institut fur Pharmakologie and Toxikologie der TU Munchen, Germany[2]; School of Pharmacy, SUNY Buffalo, Buffalo, NY[3].

DHP derivatives regulate L-type Ca^{2+} channels in a voltage-dependent manner. Neutral DHP block is promoted by depolarization and relieved by hyperpolarization, but block by charged DHP's is not relieved at negative voltages. The Modulated Receptor Hypothesis (MRH) predicts that these differences in drug action are due to restrictions in access to a common receptor domain due to the hydrophilic or hydrophobic nature of the drug molecules. Here we report molecular evidence suggesting that a positively charged headgroup added to a neutral DHP compound interacts with the $\alpha_{1c\text{-}b}$ L-type Ca^{2+} channel subunit at a site distinct from the neutral DHP high affinity binding site. L-type Ca^{2+} channels were expressed in human embryonic kidney (HEK 293) transiently-transfected with cDNA encoding wild type (WT) or mutant α_{1cb} subunits. Mutations (Y1485I, M1486F, I1493L) previously reported to markedly reduce neutral DHP binding to α_{1c} and block of expressed current (Hockerman *et al.* 1995; Schuster *et al.* 1996) were studied. We studied modulation of expressed channels by charged and neutral forms of a previously-described custom synthesized DHP with ten methylene groups separating the DHP moiety from a test neutral or charged headgroup (Bangalore *et al.* 1994). The mutations increased the IC_{50} for channel inhibition 60 fold at -40 mV (22.9 nmol/L to 1.4μmol/L) but only 8 fold when currents were elicited from -80 mV holding potentials. Charged DHP block was not affected at either at holding potential. These results associate the mutated residues with a high, but not low, affinity neutral DHP binding site, and provide strong evidence for an additional site of action for charged DHP's.

W-PM-D2

MUTATION OF IIIS5 SEGMENT OF L-TYPE CA CHANNEL MARKEDLY DECREASES THE SENSITIVITY TO DIHYDROPYRIDINES. ((**H. Ito**, N. Klugbauer and F. Hofmann)) Institut für Pharmakologie und Toxikologie der TU München, Biedersteiner Straße 29, 80802 München, Germany

The L-type voltage-gated Ca channels are the pharmacological targets of the dihydropyridines (DHP). The mechanism underlying their blocking and stimulating effect is still unclear. To answer this question, chimeras were constructed by mutating amino acids of the DHP-sensitive α1C subunit to those of the DHP-insensitive α1E subunit. The chimeras, along with β2 and α2/δ subunits, were transfected to human embryonic kidney cells and the whole-cell Ba currents were recorded. Using this strategy, we have recently shown that mutation of 3 amino acids (Tyr 1485, Met 1486, Ile 1493) in the IVS6 decreases the affinity for (+)isradipine 100-fold (Schuster *et al.* (1996), EMBO J. **15**, 2365-2370). The same method was applied to study the possible role of IIIS5 region on the DHP-sensitivity. By mutating 1 to 3 amino acids in IIIS5, the Ba currents were blocked by less than 20% by (+)isradipine at a concentration as high as 3 μM. At this concentration, the wild type α1C channel was blocked by 100%. The stimulating effect of (-)Bay K 8644 also disappeared in these chimeras. These results suggest that IIIS5 segment is critical for the DHP-sensitivity of the L-type Ca channel.

W-PM-D3

MOLECULAR BASIS OF SELECTIVE STATE-DEPENDENT INHIBITION OF CARDIAC VERSUS NEURONAL Ca CHANNELS BY DILTIAZEM ((**D.M. Cai**, J.G. Mulle, and D.T. Yue)) Molecular and Cellular Physiology Program, Dept. of Biomedical Engr., Johns Hopkins University Sch. Med., Baltimore, MD 21205

Recombinant channel techniques have revealed structural aspects of interaction between Ca channels and various therapeutic blocking agents. However, the molecular basis of state-dependent interaction, crucial for use-dependent anti-arrhythmic drugs, is less clear. Here we report that although benzothiazepines (BTZ) block recombinant C-, A-, and E-class Ca channels with only quantitative differences in potency, BTZ appear highly selective for the C-class in terms of producing state-dependent block. Upon application of diltiazem, only C-class channels showed accelerated decay of test pulse current and hyperpolarizing shifts in the $V_{1/2}$ of h_∞ curves; these features argue for state-dependent interaction. None of these effects was found with A-class and E-class channels. By contrast, phenylalkylamines (PAA) produced state-dependent block in all classes of channels. The difference in the functional effect of diltiazem upon the cardiac (C-class) versus neuronal (A- and E-class) channels gave reason to wonder whether the structures specifying state dependence are distinct from those implicated in simple binding (e.g. on domains III and IV)? We therefore examined diltiazem block of the chimeric channels CCAA and AACC, expressed in HEK 293 cells. As shown below, both chimeric channels were inhibited about 30-40% (dashed line) by diltiazem, but upon rescaling to facilitate kinetic comparison, only AACC showed clear evidence of open channel block. Like simple binding, state-dependence appears to be specified by structures localized to domains III and IV.

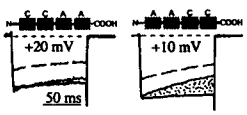

W-PM-D4

USE-DEPENDENT Ca $^{2+}$ CHANNEL BLOCK BY PHENYLALKYLAMINES (PAA): LINK BETWEEN INACTIVATION AND CHANNEL BLOCK ((**S. Hering**, E.N. Timin, S. Berjukow, S. Aczél, R. Kraus & J. Striessnig)) Institut für Biochemische Pharmakologie, Peter Mayr Straße 1, A-6020 Innsbruck, Austria (Spon. by H. Glossmann)

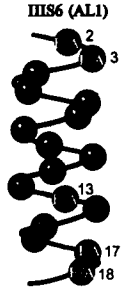

We have previously shown that transfer of only 3 amino acids of transmembrane segment IVS6 of L-type α_1 into the α_{1A} subunit (I1804Y, S1808A and M1811I) is sufficient to support use-dependent block of barium currents (I_{Ba}) by d-cis-diltiazem and (-)gallopamil (Hering et al., 1996, J.Biol.Chem. *271:* 24471-24475). These mutations in transmembrane segment IVS6 determine both, inactivation properties of calcium channels and use-dependent block of I_{Ba} by d-cis-diltiazem and (-)gallopamil. We now have studied the effect of site directed mutations in segment IIIS6 (2F/A, 3F/A, 13F/A, 17I/A, 18F/A, see figure) of a PAA-sensitive chimera AL1 (Grabner et al., 1996, Neuron, *16:* 207-218) on use-dependent block of I_{Ba} by (-)gallopamil after expression in *Xenopus* oocytes. Mutations in IIIS6 that diminished I_{Ba} inactivation simultaneously reduced use-dependent block of I_{Ba} and *vice versa*. Our data suggest a close correlation between channel inactivation and calcium channel block by PAA. The data are discussed in terms of a new model describing open channel block by PAA and drug induced inactivation.

Supported by FWF grants S6601-MED, S6602-MED and S6603-MED

W-PM-D5

MECHANISM OF PROTON BLOCK OF L-TYPE Ca^{2+} CHANNELS: THE INFLUENCE OF MUTATION OF GLUTAMATE AND AROMATIC AMINO ACID RESIDUES IN THE PORE-LINING REGION. ((**Klockner, U.**, Mikala, G., Schwartz, A., and Varadi, G.)) University of Cologne, Cologne 50931, Germany and University of Cincinnati, Ohio 45267.

Blockage of calcium channels by extracellular protons exhibits an unusual feature in that protons produce an incomplete block of the ionic current so that ionic conductance as measured by monovalent charge carriers is reduced to about one-third of its normal value. We have previously shown (Klockner et al., 1996) that a glutamate residue, located in the motif III SS2 region exhibits a uniquely high pKa value, and this site is primarily responsible for the binding of protons. The high pKa value may emerge from polar interactions with other glutamic acid residues or by repulsive free energy interactions between hydrophobic residues and carboxyl groups. Here in this study, we report the influence of neighboring aromatic amino acids and also in more detail the contribution of motif I, II, and IV SS2 glutamates, on the proton binding of Glu1086. First, we tested the influence of F1085G which surprisingly had no significant influence on the pKa value of E1086. However, mutation W1088T, another hydrophobic neighbor, decreased the pKa by 0.4 units. This phenomenon meets expectations since it was predicted that repulsive interaction from neighbor aromatic amino acid will increase the pKa of glutamates. Mutations of glutamic acid residues in each motif SS2 segment contributed by a decrease of pKa by 0.26-0.48 unit. Combined double mutations of glutamates in motifs I+IV and II+IV showed additive effects, and combination of motif III with any other motifs showed no protonated state. The behavior of triple or quadruple mutants was consistent with the observations from single or double point mutants, i.e., when motif III was present, the proton block of the channel was abolished in the pH range of 6.0-9.0. We conclude that E1086 is the single proton binding site whose affinity towards protons is strongly influenced by an intra SS2 segment tryptophan residue and spatially nearby SS2 glutamate residues.

W-PM-D6

EFFECTS OF GLU→ASP REPLACEMENT INDICATE A CONCERTED ACTION OF GLUTAMATES IN REPEATS I AND III IN FORMING THE PROTONATION SITE OF L-TYPE Ca^{2+} CHANNELS. ((X. H. Chen and R. W. Tsien)) Dept. of Mol. Cell. Physiol., Stanford, CA 94305

We have shown that the proton binding site in L-type Ca^{2+} channels is formed by conserved P-region glutamate residues (Chen, Bezprozvanny & Tsien, 1996) and proposed that the site consists of glutamate side chains from repeats I and III, acting in coordination with that from repeat II. To test this hypothesis further, we studied the effects of shortening side chain length with single Glu→Asp substitutions. When expressed in *Xenopus* oocytes, all four mutants displayed two conducting states (protonated and deprotonated), similar to wild type (WT). However, in each mutant, proton affinity and monovalent cation conductance were affected in a distinctive manner. E→D mutation in repeats I and III, but not II, caused a two-fold reduction of proton binding affinity, due to speeding of the H^+ off-rate (Figure). In contrast, E*IV*D displayed an increased proton binding affinity and a significant reduction of deprotonation rate. E→D mutations in repeats I, II, and III also significantly increased single channel conductance, especially of the protonated state of the channel. These results provide fresh support for the proposed arrangement of P-region glutamates at the locus of H^+ block.

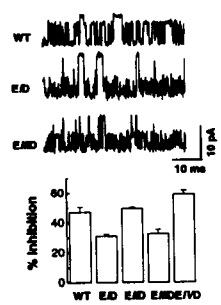

W-PM-D7

THE S5-S6 LINKER OF REPEAT I IS A CRITICAL DETERMINANT OF L-TYPE Ca^{2+} CHANNEL UNITARY CONDUCTANCE. ((R.T. Dirksen, J. Nakai, A. Gonzalez, and K. Beam)) Dept. of Neurobiol. and Anat., Colorado State University, Ft. Collins, CO 80523.

The α_1-subunits of all voltage-dependent calcium channels contain four internal homology repeats, each consisting of six transmembrane segments (S1-S6). The loops connecting the S5 and S6 segments of each repeat (S5-S6 linker) fold into the membrane and contain conserved pore-lining glutamate residues that strongly influence ion selectivity (Yang, *et al.*, 1993). In spite of a complete conservation of these pore region glutamate residues among all voltage-dependent calcium channels, the unitary conductance of the skeletal L-type calcium channel (L-channel) is nearly half that of the cardiac L-channel (~14-pS and ~25-pS, respectively). We have investigated important structural determinants of this difference in unitary conductance through single channel analysis of wild-type and chimeric skeletal and cardiac L-channels transiently expressed in dysgenic myotubes. Unitary activity was monitored from cell-attached patches in the presence of 110 mM $BaCl_2$ and Bay K 8644 (5 μM). In agreement with measurements of macroscopic currents, our results demonstrate that the composition of the first repeat determines whether ensemble averages of unitary L-channel activity display fast or slow activation. Ensemble averages activate rapidly for the purely cardiac (CARD1) L-channel and the chimeric L-channel in which only the intracellular loops (CSk9) are of skeletal origin. SkC51, in which both the intracellular loops and the S5-S6 linker of repeat I (IS5-IS6 linker) are of skeletal origin, also exhibits rapid activation. All the expressed constructs in which the IS5-IS6 linker is of skeletal origin (CAC6, SkC15, and SkC51) exhibit a low single channel conductance (~14-pS) similar to that of normal skeletal myotubes. The constructs in which the IS5-IS6 linker is of cardiac origin (CARD1 and CSk9) display cardiac-like conductance (~25-pS). These results demonstrate that the IS5-IS6 linker strongly influences the single channel conductance of skeletal and cardiac L-channels in a manner that is independent of the rate of channel activation. Supported by AR08243 (RD) and NS24444 (KB).

W-PM-D8

CLONING OF CALCIUM CHANNELS REPRESENTING TWO NEW SUBFAMILIES DISTINCT FROM HIGH VOLTAGE-ACTIVATED TYPES. ((E. Perez-Reyes, J.-H. Lee, A. Daud, and L. Cribbs)) Loyola University Medical Center, Maywood, IL 60153.

Molecular cloning studies have revealed a greater diversity of genes encoding voltage-gated channels than imagined from electrophysiological studies. To date, six calcium channel α_1 genes have been cloned, which can be grouped into two subfamilies. All of these genes encode high voltage-activated (HVA) channels. Our hypothesis is that low voltage-activated (LVA) channels are evolutionarily related to the voltage-gated channel superfamily that includes K^+, Na^+, and Ca^{2+} channels. Comparison of Na^+ and Ca^{2+} channels reveals particular areas of amino acid conservation, including transmembrane regions and pore loops. There is conservation not only between the different channels, but also between the separate domains within the channels. We have used these similarities to make PCR primers designed to amplify new channel genes. We also incorporated an evolutionary approach by including the sequences of ion channel genes from species further down the evolutionary tree. We have PCR cloned cDNA segments of channels from *Xenopus*, and even *Paramecium*. We will present evidence for four subfamilies of voltage-gated calcium channels. Considering the evolutionary expansion of the two HVA subfamilies, we predict that there may be as many as twelve genes encoding mammalian calcium channels.

NOVEL TECHNIQUES

W-PM-E1

QUANTIFYING THE CLEANLINESS OF GLASS CAPILLARIES: A FILM ON THE LUMENAL SURFACE ((C.L. Bowman[1,2])) 1. Department of Biophysical Sciences, SUNY-Buffalo 14214. 2. VAMC, Buffalo, New York 14215.

I used capillary rise methods to investigate the lumenal surface properties of quartz (Amersil T-08), borosilicate (Corning 7800), and high lead glass (Corning 0010) capillaries commonly used to make patch pipettes. I calculated the capillary rise and contact angle for water from weight measurements. The capillary rise was compared to the theoretical maximum calculated by assuming each fluid wetted the glass surface (i.e., zero contact angle which reflects the absence of surface contamination). For each type of capillary, the rise for water was substantially less than the theoretical maximum rise. Exposure to several cleaning methods resulted in better - but not perfect - agreement between the theoretical maximum rise and calculated rise. The residual discrepancy between the calculated and theoretical rise for water could not be improved upon by trying a variety of cleaning procedures, but some cleaning methods were superior to others. The water solubility of the surface contaminants, deduced from the effectiveness of repeated rinsing, was different for each of the three types of capillaries examined: Corning 7800 > quartz > Corning 0010. A surface film was also detected on quartz capillaries with an internal filament. I conclude that these capillaries have a film on the lumenal surface, which can be removed using appropriate cleaning methods. The surface contaminants are probably unique to each type of capillary, and hydrophobic. Removal of this film may reduce the glass-dependent affects on the activity of certain ion channels, and improve the frequency of successful gigaseals. A very simple method will be presented to quickly evaluate and quantitate the cleanliness of glass capillaries.

W-PM-E2

DIELECTROPHORETIC METHODS FOR CELL CHARACTERIZATION AND SORTING ((P. R. C. Gascoyne, Y. Huang, J. Vykoukal, F.F. Becker and X. - B. Wang)) University of Texas M.D. Anderson Cancer Center, 1515 Holcombe Boulevard, Houston, TX 77030)

Cells experience electrokinetic forces when subjected to an alternating electrical field as a result of the interaction between the field and field-induced polarization. The frequency responses of these forces are functions of the intrinsic cellular dielectric properties, which depend sensitively on both membrane and intracellular structure and composition. We report here two approaches for exploiting these electrokinetic effects for characterization and sorting of biological cells: (a) a spiral electrode array under phase-quadrature excitation, (b) a dielectrophoresis (DEP) based field-flow-fractionation (FFF) method. For the spiral electrode system, cell kinetic behaviors are characterized as either entrapment at electrode edges or levitation above the electrode plane and radial motion towards or away from the center of the spiral. This allows for identifying and selectively focusing rare target cell subpopulations for diagnostic applications. DEP-FFF utilizes negative DEP forces to levitate cells above parallel electrodes arrayed on the bottom of a thin chamber. A fluid-flow profile is established so as to carry cells at different equilibrium heights at different velocities. Fractionation of heterogeneous cell mixtures into subpopulations is thereby realized through velocity-differentiation by levitating cells of different dielectric properties to different heights in the flow profile. Experimental data are presented to demonstrate the principles and applications of these two approaches which are interpreted using combined hydrodynamic and generalized-DEP theories.

W-PM-E3

NEUTRON REFLECTIVITY STUDIES OF PEPTIDES IN BIOMIMETIC BILAYER MEMBRANES SUPPORTED ON PLANAR SUBSTRATES. ((S. Krueger, A. Plant, K. Meuse, C.F. Majkrzak and J. Dura)) NIST, Gaithersburg, MD 20899.

Neutron reflectivity is being used to probe the structure of peptides associated with biomimetic bilayer membranes in aqueous solution. A single hybrid bilayer membrane (HBM), consisting of one monolayer of alkanethiol and one monolayer of phospholipid, is formed on a gold-coated silicon substrate using a modified Langmuir-Blodgett technique. Since the alkanethiol monolayer is strongly bonded to the gold surface, this HBM is more rugged than a conventional supported bilayer, which binds only weakly to a silicon surface. The phospholipid monolayer is in contact with an H_2O or D_2O solution, making it possible for the HBM to support active membrane proteins. Specular reflectivity measurements are sensitive to changes in overall bilayer thickness to within 1-2Å. In addition, it is possible to determine the neutron scattering length density (SLD) profile of the HBM as a function of depth perpendicular to the bilayer surface. Since the SLD of both the lipid head group and the hydrocarbon chain are significantly different from that of most peptides, the insertion of a peptide into the bilayer would change the SLD in the layers in which it is located.

For the reflectivity measurements, an HBM of octadecanethiol and d(54)-DMPC was measured in D_2O and in D_2O containing melittin, a pore-forming toxin. Changes in the reflected intensity as a function of incident angle were clearly seen with the addition of melittin. No change in bilayer thickness was evident. Differences in the resultant neutron SLD profiles indicate that melittin penetrates at least partially into the HBM. Thus, the neutron reflectivity technique opens up the possibility of high resolution assessment of melittin penetration into this model membrane.

W-PM-E4

3D DIFFUSION MEASURED AT HIGH SPATIAL AND TEMPORAL RESOLUTION BY SCANNING MICROPHOTOLYSIS.
((Peter Wedekind, Ulrich Kubitscheck and Reiner Peters)) Institut für Med. Physik und Biophysik, Westfälische Wilhelms-Universität Münster, D-48149 Münster, Germany

Scanning Microphotolysis, a recently developed family of photobleaching and photoactivation techniques (Wedekind et al., 1994, J. Microsc. 176 23-33; Wedekind et al., 1996, Biophys. J. 71 1621-1632; Kubitscheck et al., 1996, J. Microsc. 182 225-233; Kubitscheck et al., Bioimaging, in press), was extended to three dimensional (3D) diffusion. A confocal microscope was operated in the line scan mode. By means of an accousto-optical modulator the laser beam power could be switched during scanning at pixel accuracy between high photolysing and low monitoring levels. The number, location, and length of line segments to be photolysed could freely be determined. The minimal photolysis volume had effective diameters of ~0.3 µm (FWHM in focal plane) and ~1.5 µm (optical axis) with an 40x/NA 1.0 objective. The temporal resolution was ≤0.5 ms. Together with the instrumentation a general theoretical method for the evaluation of 3D diffusion measurements based on numerical simulation by threefold time-step splitting was developed. The method could be applied to any photobleaching geometry, was suited for photobleaching by both short pulses or continuous irradiation, and took the convolution with the microscope point spread function into account. Experimental and theoretical procedures were tested by measurements on solutions of B-phycoerythrin in glycerol-water mixtures. The obtained diffusion coefficients aggreed well with expectation. First results on the diffusion of FITC-dextrans in different nuclear domains are reported. (Support by the German Research Foundation, grant Pe 138/15-4, is gratefully acknowledged)

W-PM-E5

DETERMINATION OF THE BINDING CONSTANTS OF DRUGS TO HUMAN SERUM PROTEINS AND HUMAN SERUM USING CAPILLARY ELECTROPHORESIS FRONTAL ANALYSIS

(**P. A. McDonnell** and G. W. Caldwell) R. W. Johnson Pharmaceutical Research Institute, Spring House, PA 19477

Protein binding of a drug plays an important role in pharmacokinetics and pharmacodynamics studies. The application of frontal capillary electrophoresis will be presented to determine unbound drug concentrations in drug-human serum protein binding equilibria. From these binding studies, the association constant (K_a), the maximum number of drug molecules bound to the protein and the classes of binding sites on the protein can be determined. The frontal analysis method is attractive for characterizing drug-protein binding because it utilizes a simple instrumental system, the studies are performed at conditions that approach physiological conditions and the analyses are fast.

W-PM-E6

Tuning caged calcium: NP-EGTA derivatives with improved optical and chelation properties. ((Graham C.R. Ellis-Davies)) Bockus Research Institute, Philadelphia

NP-EGTA and DM-nitrophen are Ca cages that have high affinities for Ca before photolysis and yield photoproducts with affinities in the mM range. Furthermore, Ca is released very rapidly from both cages (*BJ* **1996**, *70*, 1006). A series of derivatives of NP-EGTA has been synthesized which are designed to combine the optical properties of DM-nitrophen and the cation selectivity of NP-EGTA in one Ca cage. Principal amongst these new cages are two DM versions of NP-EGTA: DMNPE (Kd (Ca) 125 nM) and DMNPE-4 (Kd (Ca) 40 nM). These moleclues have extinction coefficients of about 4,600/M/cm (cf. 975 and 4,300 for NP-EGTA and DM-nitrophen, respectively). In a manner similar to the other Ca cages I have developed, DMNPE and DMNPE-4 are cut in two upon illumination, producing photoproducts with low affinities for Ca (mM range). Such large changes in affinity results in the release of most bound Ca. Complete physio-chemical details of these and other new Ca cages will be presented. (Supported by GM53395)

W-PM-E7

CAGED PEPTIDES AND PROTEINS.

((**Hagan Bayley**, Chung-yu Chang, Peng Pan)) Worcester Foundation, Shrewsbury, MA 01545. (Spon. by A.E. Johnson)

By using caged reagents, biologically active molecules can be generated in cells or tissues in known doses with excellent spatial and temporal control. We have developed procedures for caging cysteine or thiophosphoryl peptides and proteins at single sites with various 2-nitrobenzyl bromides. Photolysis of the caged peptides by near UV light produces uncaged molecules in $\geq$ 70% yield. Single-cysteine proteins suitable for caging are found by scanning mutagenesis or by considering structure-function analyses. By the first route, a caged pore-forming protein, for the controlled permeabilization of eukaryotic cells, has been made by derivatizing a cysteine mutant of staphylococcal α-hemolysin. By the second route, a caged catalytic subunit of protein kinase A has been obtained. The activities of many proteins involved in signal transduction are modulated by phosphorylation. Therefore, we are currently extending procedures for caging at thiophosphate from peptides to proteins.

MEMBRANE TRANSPORT

W-PM-F1

FREE ENERGY PROFILES GOVERNING H^+ CONDUCTION IN PROTON WIRES.

((R. Pomès and B. Roux)) GRTM, Départements de Physique et de Chimie, Université de Montréal, Montréal, Québec, Canada H3C 3J7

The conduction of H^+ by hydrogen-bonded chains, or proton wires, requires two complementary processes: (1) translocation of an excess proton along the hydrogen-bonded chain (propagation of a ionic defect), and (2) reorientation of the hydrogen-bonded chain in the absence of an excess proton (propagation of a bonding defect). In a previous computational study of the structure and dynamics of the proton wire of the gramicidin A (GA) transmembrane channel [Pomès and Roux, Biophys. J. 71, 19-39 (1996)], the two processes were seen to involve different time scales. In the present study, the free energy profiles for each of the two reactions are now studied separately, successively in model proton wires comprising linear chains of water molecules and in the single-file water chain filling the GA channel. Results indicate that in isolated water chains, the rapid translocation of an excess H^+ across the entire chain occurs spontaneously with thermal fluctuations, while moderate free energy barriers exist in the GA channel because of hydrogen bonding of the water molecules with the pore. In contrast, the dipole moments of the water molecules in the unprotonated chain are strongly correlated and preferentially oriented along the chain axis. Their collective reorientation involves a large free energy barrier of 7 to 8 kcal/mol in model proton wires, but only of about half as much in GA. Implications for proton conduction in biological channels are discussed.

W-PM-F2

NA-LEAK PATHWAY AND SUBSTRATE BINDING ORDER IN THE NA^+-GLUCOSE COTRANSPORTER

((**Jean-Yves Lapointe** and Xing-Zhen Chen)) GRTM, Université de Montréal, Montréal, QC, Canada H3C 3J7

The Na^+-glucose cotransporter (SGLT1) expressed in *Xenopus* oocytes was shown to generate a phlorizin-sensitive Na leak (in the absence of sugars). Using the current model for SGLT1, where the Na leak was presumed to occur after two Na ions are bound to the free carrier prior to glucose binding, a characteristic concentration constant (K_c) was introduced to describe the glucose concentration at which the Na^+-glucose cotransport current is equal to the Na leak. As both the Na leak and the Na^+-glucose cotransport current are predicted to occur after the binding of two Na ions, the model predicted that K_c should be Na-independent. However, by use of a two-microelectrode voltage-clamp technique, the observed K_c was shown to depend strongly on the external Na concentration ($[Na^+]_o$) and was four times higher at 5 mM $[Na^+]_o$ than at 20 mM $[Na^+]_o$. In addition, the magnitude of the Na leak varied as a function of $[Na^+]_o$ in a Michaelian fashion and the Na affinity constant for the Na leak was 2-4 times lower than that for cotransport in the presence of low external glucose concentrations (50 or 100 μM), whereas the model predicted a sigmoidal Na-dependence of the Na leak and identical Na affinities. These observations indicate that the Na leak occurs after one Na ion is associated with the carrier and agree with predictions from a model for which the prefered binding order is Na:Glucose:Na. This conclusion was also supported by experiments performed where protons replaced Na^+ as a driving cation.

W-PM-F3

NOVEL FUNCTIONAL DIFFERENCE BETWEEN *DROSOPHILA* AND HUMAN Na^+/Ca^{2+} EXCHANGERS ((A. Ruknudin[1,2], W.J. Lederer[2,3] and D.H. Schulze[1])) Departments of [1]Microbiology & Immunology, [2]Physiology, [3]Molecular Biology & Biophysics, University of Maryland at Baltimore, Baltimore, MD. 21201 USA.

We have cloned cDNA for *Drosophila* Na^+/Ca^{2+} exchanger (Dmel/Ncx) by homology screening using human heart Na^+/Ca^{2+} exchanger cDNA. The deduced protein structure from the sequence shows two sets of six potential transmembrane domains with an intracellular region in between as seen in mammalian exchangers. The first set of transmembrane contain a cleavable signal peptide as seen in the mammalian Na^+/Ca^{2+} exchangers. The overall sequence comparison of Dmel/Ncx to the mammalian Na^+/Ca^{2+} exchangers is about 44% at the amino acid level. The most conserved regions are observed in the putative transmembrane domains (~66.2%)and lesser conservation is seen in the intracellular loop region (~33.8%). Since the primary structure of Dmel/Ncx varied considerably from the known mammalian sequences we looked for the differences in their function. cRNAs for human cardiac (NCX1) and *Drosophila* exchangers were injected into Xenopus oocytes and the function was assayed by Na-dependent ^{45}Ca influx. The oocytes injected with Dmel/Ncx exchanger cRNA showed a Ca^{2+} influx of 3.23 +0.43 pmoles per oocyte per 10 min., a 20 fold increase over water-injected oocytes. 4 mM $NiCl_2$ reduced this Na-dependent Ca^{2+} influx by 17 fold. In this way, Dmel/Ncx functioned like other mammalian exchangers. But it differed with regard to Ca^{2+} transport in Ca^{2+}-Ca^{2+} exchange and the effect of monovalent-dependent Ca^{2+}-Ca^{2+} exchange. Under identical conditions, the unidirectional Ca^{2+} flux through the *Drosophila* exchanger was 0.12+0.02 pmoles/oocyte, 3.6-fold lower than human exchanger in the presence of extracellular Na^+. One kinetic feature that could explain the difference between these exchangers is Ca^{2+}-self exchange or Ca^{2+}-Ca^{2+} exchange. To explore further, under conditions which should favor efflux of Ca^{2+} by Na^+-gradient, isotopic Ca^{2+} influx was measured. The influx of Ca^{2+} in *Drosophila* was 0.66+0.02 pmoles/oocyte, a 5-fold decrease when compared to the human exchanger confirming that the rate of Ca^{2+}-Ca^{2+} exchange in *Drosophila* is lower. The Ca^{2+} flux via Ca^{2+}-Ca^{2+} exchange through these exchangers was suppressed by La^{3+}. This suggests that some kinetic features of *Drosophila* Na^+/Ca^{2+} exchanger that involves Ca^{2+} movement are different from human Na^+/Ca^{2+} exchanger.

W-PM-F4

PROTON AND HYDROXIDE DECAY KINETICS IN BUFFERED VESICLES ((J.A. Novotny, S. Metzger, M. Gawienowski, D. Briskin and **J. Whitmarsh**)) Diet and Human Performance Laboratory, USDA/Agricultural Research Service, Beltsville, MD 20705, Center of Biophysics and Computational Biology and Department of Crop Sciences, University of Illinois, Photosynthesis Research Unit, USDA/Agricultural Research Service, Urbana, IL 61801. (Spon. by J. Whitmarsh)

The problem of predicting the kinetics of the decay of the internal proton concentration for vesicles containing one or more buffers and for which a pH gradient exists across the membrane is examined. The solution builds on earlier work describing proton efflux (J. Whitmarsh (1987) Photosynth. Res. 12:43-62) that was successfully applied to chromatophores from *Rhodobacter capsulatus* (M.P. Turina, G. Venturoli & B. Melandri (1990) Eur. J. Biochem. 192:39-47). An analytical solution is derived that describes the time course of the proton efflux and hydroxyl influx and the internal proton concentration under conditions of zero transmembrane electric potential. The effect of the internal buffers is to increase the time required for the proton/hydroxyl gradient to equilibrate across the membrane. For a vesicle containing a single buffer the solution requires 7 independent physical parameters: the initial internal proton concentration, the external proton concentration, the ratio of the vesicle surface area to the internal volume, the permeability coefficients of the membrane for protons and for hydroxyl ions, the total concentration of the internal buffer, and the equilibrium constant for the dissociation of the internal buffer. Determination of these physical values is sufficient to predict the time dependence of the internal proton concentration and of the proton/hydroxyl ion efflux and influx. The theory is applied to plant vacuoles and accounts for the long life (many hours) of pH gradients observed across the tonoplast membrane in the apparent absence of active transport.

W-PM-F5

PROTEIN HALF-LIFE AND ANTISENSE INHIBITION OF THE Na/Ca EXCHANGER IN PRIMARY CULTURED NEONATAL RAT CARDIOMYOCYTES. ((M.K. Sladzinski and M.P. Blaustein)) Physiol. Dept., U. of Maryland Med. Sch. Baltimore, MD 21201

The cardiac Na/Ca exchanger (NCX) has been well characterized. Here, we describe the NCX protein half-life in primary cultured neonatal rat cardiomyocytes, and physiological and biochemical evidence of NCX inhibition by antisense oligodeoxynucleotides (AS-oligos) targeted to the NCX1 transcript. Protein half-life was determined using [^{35}S] methionine with a pulse-chase protocol. Labeled NCX protein was immunoprecipitated and Western blotted. The ^{35}S-NCX signal was localized to the NCX protein band and normalized using densitometry. The NCX protein half-life was 33 hrs. For antisense experiments, we employed AS-oligos previously studied in vascular smooth muscle (*AJP* 269:C1340, 1995). AS-oligo treated cardiomyocytes were morphologically indistinguishable from control (no oligos) and scrambled oligo (NS-oligo) treated cells. Cytosolic free Ca^{2+} concentrations ($[Ca^{2+}]_{cyt}$) were measured with digital imaging in fura-2 loaded cells. All cells in which 50 mM external K^+ evoked a reversible rise in $[Ca^{2+}]_{cyt}$ were considered viable, and were studied (AS-oligo as well as control and NS-oligo treated). All control and NS-oligo cells but, after 4 days in culture, only about 50% of AS-oligo cells exhibited a rise in $[Ca^{2+}]_{cyt}$ when external Na^+ was removed. The latter cells (with NCX knock down) were the only ones that exhibited a rise in $[Ca^{2+}]_{cyt}$ when the cells were superfused with caffeine (CAF) and cyclopiazonic acid (CPA) to unload SR Ca^{2+} stores. Spontaneous Ca^{2+} transients were observed in all controls and NS-oligo cells, but not in the ≈50% of AS-oligo cells with NCX knockdown after 4 days in culture. At days 1 and 7, NCX protein concentration was determined by Western blot and densitometry. At day 7, AS-oligo treated cells had ≈50% less NCX protein than control and NS-oligo treated cells; no differences were noted at day 1. The NCX protein 33 hr half-life correlates well with the time course of AS-oligo knock down of NCX protein and function.

W-PM-F6

SUBSTRATE BINDING AFFINITY OF THE OXALATE TRANSPORTER (OXLT) DETERMINED USING CIRCULAR DICHROISM SPECTROSCOPY ((DaXiong Fu & Peter C. Maloney)) Department of Physiology, Johns Hopkins Medical School, Baltimore, MD 21205

OxlT, an antiporter catalyzing oxalate/formate exchange in *Oxalobacter formigenes*, is a member of a large family of transporters that display the reactions of antiport, uniport or symport. Circular dichroism spectroscopic analysis of the purified histidine-tagged variant, OxlTHis, revealed a dominant profile of α-helical structure, encompassing 60-70% of OxlTHis residues. The α-helical structure showed a clear substrate-dependent stability. At 37 °C, the ellipticity at 222 nm (Θ_{222}) of the unliganded OxlTHis decayed spontaneously with a time constant of 3 min, whereas that of the fully liganded OxlTHis remained unchanged for hours. The decay rate constant ratio of Θ_{222} in the presence to absence of oxalate is thus governed by the oxalate occupancy. Least-squares fitting of the ligand occupancy to a Hill equation gave a binding affinity of 9.7 ± 1.7 μM and a Hill coefficient of 1.1 ± 0.2, suggesting a 1:1 binding stoichiometry. Consistent with previous functional studies, our results now also reveal a quantitative structure-function relationship between the α-helical content and activity of this membrane transporter.

W-PM-F7

ELECTROPHYSIOLOGICAL ANALYSIS OF THE HUMAN CREATINE TRANSPORTER. ((W. Dai,[1] D.L.Kunze,[2] and **H.K.Sarkar**,[1])) [1]Baylor College of Medicine, Houston, TX 77030 and [2]Rammelkamp Center for Education and Research, Cleveland, OH 44109.

We examined the electrophysiological properties of the human heart creatine transporter expressed in *Xenopus* oocytes using two-electrode voltage-clamp technique. Application of creatine in NaCl buffer induced a steady-state inward current in creatine transporter RNA injected oocytes but not in uninjected oocytes. In the absence of creatine, depolarization induced a transient current in the injected oocytes incubated in NaCl buffer. The transporter expression level was correlated with the magnitude of the transient current. The transient current was dependent on membrane potential and external Na^+ concentration, influenced by external Cl^- concentration to a lesser degree, and inhibited by external creatine. The data suggest that the transient current originates from the interaction of Na^+ with the transporter and that this interaction is regulated by both voltage and binding of Cl^-.

This work was supported by AHA Grant-in-Aid No. 95012190.

W-PM-F8

THE FUNCTIONAL CHANGE OF THE MITOCHONDRIAL PHOSPHATE CARRIER FROM COUPLED ANTIPORT TO UNCOUPLED UNIPORT DEPENDS ON THE PRESENCE OF A SINGLE CYSTEINE RESIDUE. ((**R. Kraemer**, A. Schroers, K. Herick, H. Wohlrab)) IBT 1, Research Center Juelich, Germany and BBRI Boston, USA (Spon. by H. Wohlrab)

The mitochondrial phosphate carrier (PIC) in its physiological function catalyzes both Pi^-/Pi^- and Pi^-/OH^- exchange(1). We showed that this carrier can undergo a functional shift from coupled antiport to uncoupled uniport after modification of (two) cysteine residues (2). The new transport mode has retained most of its carrier properties (rate constants, activation energy, kinetic trans-effect), however, it has lost its substrate specificity at the internal binding side of the protein. In order to address this question on the molecular level we have used the PIC from yeast (*S. cerevisiae*) mitochondria, which was heterologously expressed in *E. coli*, solubilized, purified and reconstituted (3). From the three cysteine residues present in the yeast PIC at positions 28, 134 and 300, only one single cysteine residue (C28) is responsible for this functional switch. After replacement of C28 by serine, the functional interconversion was blocked. The consequences of this finding for structural properties of the dimeric PIC carrier are discussed. After incorporation of the PIC into giant liposomes, electrophysiological methods (patch-clamp) can be used to study the properties of the carrier protein. Under these conditions the membrane-embedded phosphate carrier behaves as an anion-selective channel, which can reversibly be blocked by phosphate.

(1) Stappen, R. and Kraemer, R. (1994) J. Biol. Chem. 269, 11240-11246
(2) Stappen, R. & Kraemer, R. (1993) Biochim. Biophys. Acta 1149:40-48
(3) Wohlrab, H. & Briggs, C. (1994) Biochemistry 33:9371-9375

W-PM-F9

TISSUE SPECIFICITY OF THE CARDIAC SODIUM-CALCIUM EXCHANGER PROMOTER . ((**S.B. Nicholas**, H. Zhu, J. Lytton, K.D. Philipson)) UCLA School of Medicine, Los Angeles, CA 90095 and Univ. of Calgary (Spon. by D.A. Nicoll).

The sodium-calcium exchanger (NCX1) is intimately involved in maintaining calcium homeostasis in the heart as well as other tissues. The cardiac transcription start site of NCX1 has been identified by 5'RACE and verified by RNase protection assay and Northern Blot analysis (Lee et al., *JBC* 269:14849, 1994). In these experiments, a series of transfection assays were used to analyze the activity of rat genomic DNA fragments containing the cardiac transcription start site. The results classify this DNA as the NCX1 promoter and is cardiac tissue-specific.
The DNA used included a 3.6kb DNA fragment and an overlapping smaller 421bp DNA fragment which contained 325bp upstream from the cardiac transcription start site. Both DNA fragments were ligated into the pGL2Basic promoter-less vector containing the luciferase reporter gene to form pGL23.6 and pGL2H, respectively. For comparison, pRSV (Rous Sarcoma Virus) with a strong SV40 enhancer provided maximum tissue non-specific promoter activity and pMLC (Myosin Light Chain) provided cardiac tissue-specific promoter activity. Primary (1°) cardiac myocytes from 24-48° old Sprague-Dawley rats, CHO (Chinese Hamster Ovary) and COS-7 (African Green Monkey kidney) cells were transfected.
Promoter activity of pMLC, PGL23.6 and pGL2H was significantly higher in 1° myocytes than any other cell type ($p<0.05$). In addition, activity of pGL2H was 3 times higher in 1° myocytes than activity of pGL23.6 and 1.5 times higher than pMLC. Activity of pGL2Basic was minimal in all cell types.
Successive truncations of pGL2H to 321bp, 221bp and 121bp fragments revealed that "basal" NCX1 promoter activity resides in the 221bp fragment which contains only 125bp upstream from the cardiac transcription start site.

PHOTOSYNTHESIS III

W-PM-G1

DIRECT EVIDENCE FOR INTEREXCITON-STATE RELAXATION IN ALLOPHYCOCYANIN. ((**Maurice D. Edington**, Ruth E. Riter, William M. Diffey and Warren F. Beck)) Department of Chemistry, Vanderbilt University, Nashville, TN 37235.

We have obtained direct evidence for ultrafast interexciton-state relaxation processes at room temperature in the cyanobacterial light-harvesting protein allophycocyanin using femtosecond transient hole-burning (THB) spectroscopy with variable wavelength excitation. Interexciton-state relaxation between the two states of the α84–β84 tetrapyrrole dimers in allophycocyanin occurs on the 10–30-fs time scale, as evidenced by the production of *hole-burned* line shapes to the red of the pump spectrum. On the < 300-fs time scale, we observe line broadening owing to intramolecular vibrational redistribution and vibrational relaxation processes that occur subsequent to population of the lower exciton state. On the 300-fs–2-ps time scale, the THB spectra exhibit a time evolution arising from exciton localization. The results of this study suggest the possibility that coupled chromophore dimer structures in photosynthetic light-harvesting proteins are afforded extremely rapid radiationless transfers of population from upper to lower exciton states, with localization processes following on a longer time scale. We are interested in the possibility that these processes augment the natural energy-funneling process associated with long-distance Förster energy transfer between light-harvesting proteins and photosynthetic reaction centers.

W-PM-G2

CRYSTALLIZATION OF *MASTIGOCLADUS LAMINOSUS* CYTOCHROME b_6f COMPLEX, AND OF THE *p*-SIDE DOMAIN OF THE CHLOROPLAST RIESKE PROTEIN ((D. Huang[1], H. Zhang[1], J. M. Krahn[1], C. J. Carrell[1], G. M. Soriano[1], V. Sled[2], T. Ohnishi[2], J. L. Smith[1], and **W. A. Cramer**[1])) [1]Dept. of Biol. Sci., Purdue Univ., W. Lafayette IN 47907; [2]Dept. of Biochem. & Biophys., Univ. of Penn., Philadelphia, PA 19104. (Spon. by M. G. Rossmann)

Cytochrome b_6f complex has been isolated as an M_r ~200,000 dimer from the thermophilic cyanobacterium *M. laminosus*. The complex contains the four major polypeptides, cytochrome *f*, cytochrome b_6, the Rieske [2Fe-2S] protein, and subunit IV, and has a very high activity for electron transfer from decylplastoquinol to oxidized plastocyanin (435 cyt $f^{-1}sec^{-1}$ at 32°C). The heme ratio of cyt b_6 to cyt *f* is 2:1, and there is one chlorophyll *a* per monomer with λ_{max}=671 nm. Red-brown single crystals (0.1x0.15x0.25mm) have been obtained, by vapor diffusion from hanging drops at 20°C, that diffract X-rays regularly to 20Å. The unit cell dimensions are ~285Åx135Åx135Å, and imply a trigonal symmetry.

A soluble, 139 residue C-terminal polypeptide of the Rieske [2Fe-2S] protein of the b_6f complex was obtained by limited proteolysis. The reduced-oxidized optical difference spectrum was used to determine the E_m, +359±7mV at 25°C from pH 5.5-6.5, and +319±2mV at pH 7, with pK_{ox}=6.5±0.2 for the oxidized protein. The EPR spectrum has g values, g_z=2.03, g_y=1.90, and a broad band at g_x=1.74, similar to those in the b_6f complex. From EPR at 17°K, E_m=+365-375mV of the Rieske fragment, and +295-300mV in the cyt b_6f complex, at pH 6 and 7, implying that the cluster environment in the fragment is slightly more polar than in the complex. Single crystals of the Rieske polypeptide diffract X-rays to <2.5Å, contain 1 molecule/asymmetric unit, have a solvent content of 30%, and belong to triclinic space group P1 with unit cell dimensions, a=29.1Å, b=31.9Å, c=35.8Å, α=95.6°, β=107.1°, γ=117.3°. [NIH GM38323, USDA 95-37306-2045]

W-PM-G3

ELECTRON AND PROTON TRANSFER RESOLVED IN THE ELECTROCHROMISM ASSOCIATED WITH QUINONE REDUCTION IN BACTERIAL REACTION CENTERS. ((**D.M. Tiede**[1], D.M. Gallo[2] and D.K. Hanson[3])) [1]CHM and [3]CMB Argonne National Laboratory, Argonne, IL 60439 and [2]Augustana College, Rock Island, IL 61201.

We have measured the electrochromic response of the bacteriopheophytin, Bph, and bacteriochlorophyll, Bchl, cofactors during the $Q_A^-Q_B \rightarrow Q_AQ_B^-$ electron transfer in reaction centers, RCs, from *Rb. capsulatus* and *Rb. sphaeroides*. Measurements were made with RCs in chromatophores and in detergent-isolated states, using both antennaless and LHI containing strains. The $Q_A^-Q_B \rightarrow Q_AQ_B^-$ electron transfer is significantly faster in chromatophores than in isolated RCs. The chromatophore spectra can be interpreted in terms of a rapid electrochromic response arising from biphasic electron transfer, with risetimes of about 4 μs (70%) and 40 μs (30%) in *Rb. capsulatus* and 5 μs (65%) and 80 μs (35%) in *Rb. sphaeroides*. The magnitude of the Bph electrochromism associated with the initially formed Q_B^- state is comparable to that for Q_A^-. Subsequent, partial attenuation of the Q_B^- electrochromism occurs with a time constant of 100 μs - 300 μs. This can be attributed to partial charge compensation by H^+(or other counter ion) movement into the Q_B pocket. The amplitude of this movement appears to vary with the bacterial strain and condition of the chromatophore. The electron transfer events are slower in isolated RCs, and overlap H^+ transfer, although measurements show that the electron and proton transfer processes can be separated at low temperature (< -20° C). DOE, Offices of Basic Energy Sci., Div. Chem. Sci., and of Health and Env. Research, contract W-31-109-Eng-38.

W-PM-G4

STRUCTURE OF THE *Rb. sphaeroides* REACTION CENTER-CYTOCHROME C_2 COMPLEX IN SOLUTION. ((**D.M. Tiede**[1], P.A. Marone[1] and P. Thiyagarajan[2])) [1]Chemistry Division and [2]Intense Pulsed Neutron Source, Argonne National Laboratory, Argonne, IL 60439 (Spon. by P. D. Laible)

We have used Small Angle Neutron Scattering, SANS, to characterize the structure of the *Rb. sphaeroides* reaction center-cytochrome c_2 complex in solution, and to correlate its structure with electron transfer characteristics. Scattering from the solubilizing detergent was minimized by using deuterated reaction center and cytochrome proteins, and by using $^2H_2O/^1H_2O$ ratios that were contrast matched to the detergent. Reaction center-cytochrome c_2 preparations that exhibited simple, single exponential electron transfer kinetics were found to have a particle volume matching a 1:1 binding stoichiometry, and to have a structure consistent with a low resolution x-ray structure determined from co-crystals [Adir et al, 1996 Biochem. 35: 2535]. An alternate structure derived from electrostatic minimization of this model did not fit the solution scattering data. Reaction center preparations exhibiting more complex electron transfer kinetics, described by "proximal / distal" cytochrome binding sites in the literature, were found to have a markedly different solution structure. The volume of these reaction center-cytochrome c_2 particles considerably exceeded that of a simple 1:1 complex, and possibly arose from dimeric reaction centers. These results suggest that reaction center aggregation is responsible for the variation in kinetics reported in the literature, and provide evidence that the model for the 1:1 complex in co-crystals is relevant to the solution environment. DOE, Offices of Basic Energy Sci., Div. Chem. Sci. contract W-31-109-Eng-38.

W-PM-G5

DYNAMIC ENERGY LOCALIZATION IN BACTERIAL ANTENNA COMPLEXES: THE INFLUENCE OF NUCLEAR MOTION ON THE MECHANISM OF EXCITATION TRANSFER ((**R. Kumble**, S. Palese, R. W. Visschers, P. L. Dutton and R. M. Hochstrasser)) Department of Chemistry and the Johnson Research Foundation, University of Pennsylvania, Philadelphia, PA 19104.

Ultrafast pump-probe spectroscopy has been applied to follow excitation dynamics within the core antenna complex (B873) from *Rs. rubrum* and its dimeric subunit (B820) in the visible, near-infrared and infrared spectral regions. These measurements have revealed fast relaxation processes within the dimeric subunit which imply a strongly scattered mechanism for excitation transfer amongst the bacteriochlorophyll (BChl) pigments within the antenna aggregates: both the Stokes shift and dephasing between the BChl dimer exciton levels of B820 occur on a sub-50 fs timescale. Transient spectral properties in the near-IR and IR regions have been studied to gain insight into (a) the detailed exciton level structure of antenna complexes from location of inter-exciton and charge-transfer transitions; (b) contributions of static and dynamic localization phenomena from monitoring the evolution of vibrational difference spectra in the 1600-1750 cm^{-1} range. The relevance of vibrational properties in understanding the mode of energy transfer will be discussed, elaborating upon the information obtained from the observation of coherent wavepacket states and from transient infrared measurements.

W-PM-G6

CHEMICAL COMPLEMENTATION IDENTIFIES A PROTON ACCEPTOR OF REDOX-ACTIVE Y_D IN PHOTOSYSTEM II.
((**Sunyoung Kim**, Richard J. Debus, and Bridgette A. Barry)) Dept. of Biochemistry, University of Minnesota, St. Paul, MN 55108 and Dept. of Biochemistry, University of California, Riverside, CA 92521

Photosystem II (PSII) contains a stable, light-induced, deprotonated tyrosine radical, $D^{\bullet}$. Using site-directed mutagenesis and chemical rescue, we have identified a proton acceptor for redox-active tyrosine D. Effects of mutagenesis and chemical rescue on the proton acceptor were monitored by difference FT-IR spectroscopy, and effects on the tyrosyl radical were monitored by EPR spectroscopy. We have acquired a vibrational spectrum associated with oxidation of tyrosine D and the protonation of the acceptor. The 3600-3100 cm^{-1} region of the spectrum contains N-H stretching vibrations, demonstrated by isotopic labeling. Mutagenesis of histidine 189 of D2 to leucine (HL189D2) alters the FT-IR and EPR spectra. In attempt to biochemically complement side-chain function, imidazole or 4-methylimidazole was then reconstituted into HL189D2 PSII. Both FT-IR and EPR spectra of imidazole-reconstituted samples support the conclusion that an accessible cavity has been generated in the mutant and that functional reconstitution has occurred. Imidazole-reconstituted samples showed an increase in $D^{\bullet}$ yield that is consistent with reconstitution in approximately 40% of centers. The FT-IR spectrum of 4-methylimidazole-reconstituted HL189D2 samples demonstrates that this species does not act as a reversible proton acceptor/donor partner for the radical; this result may be due to either the larger steric bulk or higher basicity of 4-methylimidazole, as compared to imidazole. We conclude that histidine 189 of D2 acts as a proton acceptor for redox-active tyrosine D.

W-PM-G7

A DIFFERENCE INFRARED STUDY OF THE PHOTOSYNTHETIC WATER-OXIDIZING COMPLEX
((**Jacqueline J. Steenhuis** and Bridgette A. Barry)) Department of Biochemistry, University of Minnesota, St. Paul, MN 55108

We have studied the two forms of the S_2 state of the manganese-containing catalytic site of photosystem II using difference infrared spectroscopy. With this method we can test the hypothesis that there are protein conformational differences between the two forms of the S_2 state, which are known as the g=4.1 and the multiline state. A light-minus-dark difference spectrum was constructed at 200 K, 130 K, and 80 K. These illumination temperatures generated the S_2 multiline state, the S_2 g=4.1 state, and a chlorophyll cation radical, respectively. Our data show that the g=4.1 form of the S_2 state arises from a unique protein conformation. Also, these spectra show that formation of the S_2 multiline state perturbs the vibrational spectrum of a carboxylic acid residue. This residue may be in the vicinity of the manganese cluster. A change in hydrogen bonding or effective dielectric constant upon formation of the S_2 state can explain this perturbation. This carboxylate residue is conserved in cyanobacterial and plant photosystem II.

K-ATP CHANNELS

W-Pos1

AGONIST-INDEPENDENT, GTP-MEDIATED STIMULATION OF CARDIAC K_{ATP} CHANNELS. ((A.Babenko and G.Vassort)) INSERM U390, Montpellier 34090 FR.

Hypothesis on agonist-dependent $G_{i,o}$ protein-mediated activation of cardiac K_{ATP} channels via membrane-delimited mechanism is based on observations that GTP added to ATP-containing solution bathing inside-out patches in the presence of adenosine or acetylcholine at the outer side of membrane and application of $G_{\alpha i-1,2}$ and $G_{\beta\gamma}$ subunits increase the channel open probability (NP_o). We report now that GTP stimulates K_{ATP} channels in inside-out sarcolemma fragments from rat ventricular cells under similar experimental conditions but without any agonist added to the pipette solution. The probability of observation of the GTP-induced K_{ATP} channels stimulation and relative

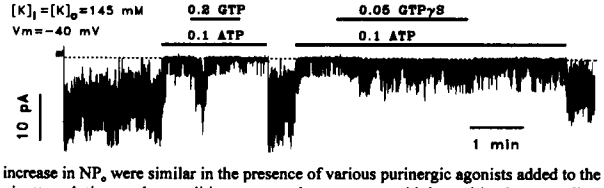

increase in NP_o were similar in the presence of various purinergic agonists added to the pipette solution, under conditions expected to prevent rapid desensitization as well as uncontrolled presence of ATP at the outer side of patches due to possible ATP transport from "intracellular" solution, and/or P_1-purinoceptor activation by adenosine derived from ATP hydrolysis. The effect was not inhibited by pertussis and cholera toxins treatment. In conclusion, GTP stimulates K_{ATP} channels independently of extracellular agonists via a membrane-delimited $G_{i,o}$ protein-independent mechanism. Supported by RFBR.

W-Pos2

BIOPHYSICAL CHANGES OF SKELETAL MUSCLE K_{ATP} CHANNELS IN K^+ DEPLETED RATS AND PHARMACOLOGICAL INTERVENTIONS.
((D. Tricarico, R. Mallamaci, V. Tortorella* and D. Conte Camerino)) Dept. of Pharmacobiology, and Dept. of Medicinal Chemistry*, Faculty of Pharmacy, University of Bari, Bari, ITALY.

Recently, mutations in the gene encoding the α1-subunit of the skeletal muscle Ca^{2+}-channel have been found in patients affected by hypokalemic periodic paralysis (HOPP) (Sipos et al., *J.Physiol.* 483.2:299, 1995). However, the link between the fiber depolarization, the paralysis and the Ca^{2+} channel mutation is still obscure. The administration of ATP sensitive K^+ channels (K_{ATP}) openers, pinacidil and cromakalim, to HOPP patients prevents the muscle paralysis. In the present work we investigated the properties of K_{ATP} channels of skeletal muscle fibers of K^+ depleted rats (Hypo K^+), the animal model of HOPP. In these rats, we tested cromakalim, and vanadate and mexiletine, drugs that have been shown to open K_{ATP} channels of cardiac cells. A treatment of male Wistar rats with K^+ free diet for 38-45 days led to a drop of serum K^+ level from 5.0±0.1 meq/L in the normokalemic rats (normo K^+) to 2.6±0.2 meq/L in the Hypo K^+ rats. In these animals, the resting potential of the extensor digitorum longus (EDL) muscle fibers of the Hypo K^+ rats, recorded by the two microelectrode technique, was drastically reduced. Further depolarization occurred after "in vivo" and "in vitro" administration of insulin. Similar phenomenas occurs in HOPP patients. Patch clamp recordings, showed that the mean current of K_{ATP} channel was reduced in the Hypo K^+ rats. Two types of K_{ATP} channels have been found in the Hypo K^+ rats. The first type, had a low single channel conductance (γ) of 29±4 pS. Whereas, γ was 71±1 pS in the normo K^+ rats. The second type had a K_{ATP} channel with normal γ but an altered selectivity to K^+ ion. Both types of channels partially lost the sensitivity to both MgATP and MgADP. Cromakalim (10-100 μM), vanadate (500 μM) and mexiletine (100-500 μM) restored the K_{ATP} conductance and prevented the fiber depolarization induced by insulin in Hypo K^+ rats. Our data indicate that closure of K_{ATP} channels contributes to the fiber depolarization in the Hypo K^+ rats, and that this animal model is suitable to search for therapeutic strategies in HOPP. (Telethon-Italy, project n° 579).